Energy & Environmental Science

Cite this: *Energy Environ. Sci.*, 2011, **4**, 1113

www.rsc.org/ees

REVIEW

Graphene based new energy materials

Yiqing Sun, Qiong Wu and Gaoquan Shi*

Received 18th November 2010, Accepted 22nd December 2010
DOI: 10.1039/c0ee00683a

Graphene, a one-atom layer of graphite, possesses a unique two-dimensional (2D) structure, high conductivity and charge carrier mobility, huge specific surface area, high transparency and great mechanical strength. Thus, it is expected to be an ideal material for energy storage and conversion. During the past several years, a variety of graphene based materials (GBMs) have been successfully prepared and applied in supercapacitors, lithium ion batteries, water splitting, electrocatalysts for fuel cells, and solar cells. In this review, we will summarize the recent advances in the synthesis and applications of GBMs in these energy related systems. The challenges and prospects of graphene based new energy materials are also discussed.

1. Introduction

Graphene, a single layer graphite with close-packed conjugated hexagonal lattices, is recognized as the basic building block of all-dimensional graphitic materials.[1,2] This unique structure endows graphene with various superior properties such as high electrical and thermal conductivities,[1,3,4] good transparency,[5] great mechanical strength,[6] inherent flexibility and huge specific surface area (SSA).[7] Therefore, graphene has attracted a great deal of attention during recent years in the fields of microelectronic and optoelectronic devices,[2,8,9] energy storage materials,[7,10,11] electrocatalysts,[12,13] polymer composites,[14] and ultrastrong paper-like materials.[15–18] Moreover, functional graphene can be prepared through low-cost solution-based processes,[19] leading to an attractive commercial application prospect.

In the 21st century, aggravating energy and environmental problems such as pollution, fossil fuel depletion and global warming are ringing the alarm bell to human society. Therefore, clean and renewable energy materials as well as their devices are urgently demanded. The utilization of renewable energy consists of two steps. First, energy can be effectively converted to applicable forms (electricity or fuel) from infinite sources, especially from solar power and water. Aiming at this goal, solar cells, fuel cells and water splitting are mostly concerned.[20–24] Second, high-performance energy storage devices are also required. This is mainly due to the intermittent characteristics of most renewable energy sources. Lithium ion batteries and supercapacitors are most promising devices for this purpose.[22,25,26] On the basis of its unique structure and excellent properties, graphene is a promising material for applications in the energy-related systems described above.[27–35] Examples include the use of GBMs as

Department of Chemistry, Tsinghua University, Beijing, 100084, People's Republic of China. E-mail: gshi@tsinghua.edu.cn

Broader context

The developments of energy storage and conversion techniques strongly depend on the achievements of material science. Graphene, a one-atom-thick carbon sheet discovered by Geim and co-workers in 2004, possesses superior electronic, thermal, and mechanical properties attractive for a wide range of potential applications. A variety of different methods have been developed to produce graphene sheets and their functionalized derivatives or composites. Among them, mechanical exfoliation, epitaxial growth, and chemical vapor deposition can produce high-quality graphene sheets desirable for fundamental studies and advanced electronic or optoelectronic devices. On the other hand, the production of graphene sheets by oxidative exfoliation of graphite can offer the high-volume production of graphene derivatives (*e.g.*, graphene oxide and reduced graphene oxide). Furthermore, functionalized graphene materials are processable and can be assembled into various desired macroscopic architectures or blended with other nanomaterials into functional composites. This review paper summarizes the different methods of producing GBMs for applications in supercapacitors, solar cells, lithium ion batteries, electrocatalysts for fuel cells and water splitting. These new carbon energy materials have also been compared with other carbon nanomaterials such as carbon nanotubes, fullerene derivatives and carbon black. This review addresses the current limitations, technical and economical viability of these new materials, and indicates their potentials in renewable energy technologies.

transparent conductive electrodes or active materials in solar cells,[36,37] counter electrodes in dye-sensitized solar cells,[38,39] electrocatalysts for oxygen reduction in fuel cells,[40–42] photocatalysts in water splitting,[43–45] and high-performance electrodes in supercapacitors[7,10] and lithium ion batteries.[11,46,47] This review mainly focuses on the recent advancements on the synthesis of GBMs and their applications in energy related systems.

2. Preparation of GBMs

2.1 Graphene

The first piece of graphene sheet was obtained *via* manual mechanical cleavage of graphite with a Scotch tape.[1] The exfoliated graphene manifests a unique structure and superior properties, although this production method is not applicable on a large scale. Inspired by this pioneering work, several alternative techniques have been developed for fabricating graphene materials.[48] For fabricating GBMs used in energy related techniques, four methods have mostly been exploited and summarized here. First, high-quality large-area graphene sheets can be prepared by epitaxial growth on single-crystal SiC[49,50] or chemical vapor deposition (CVD) on metal foil surfaces.[51,52] These graphene films can be easily transferred to arbitrator substrates by etching away the metal supports.[53] This method has been widely used to prepare high-quality graphene-based transparent electrodes for solar cells as well as other optoelectronic devices.[54] Besides, if polycrystalline SiC granules were used as a reactant for thermo-splitting, a bulk quantity of graphene sheets were obtainable while their lateral sizes were limited to several hundred nanometres.[55] The second approach is the oxidation–exfoliation–reduction of graphite powder.[19,56,57] Severe oxidation treatment converts graphite to hydrophilic graphite oxide which can be exfoliated into single-layer graphite oxide (graphene oxide) *via* stirring or mild sonication in water. Graphene oxide can be regarded as a functionalized graphene containing hydroxyl, epoxy and carboxylic groups, providing reaction sites for chemical modifications.[58] Reducing graphene oxide can partly restore its graphitic structure as well as conductivity.[59] Although reduced graphene oxide (r-GO, also called chemically modified graphene (CMG), chemically converted graphene (CCG) or graphene) has considerable defects, it is one of the most widely used GBMs as renewable energy materials due to its lowest cost, facile preparation process, large productivity, and potential for functionalization. The third strategy is directly exfoliating graphite *via* sonication,[60,61] intercalation[62,63] or quenching.[64] The resulting graphene materials have much fewer defects than those of r-GO. However, this method is not widely used because of its elaborate procedures, unsatisfactory yield of single layer graphene or sonication induced scissoring of graphene sheets into very small sizes. Last but not least, nanosized graphene can be synthesized *via* organic coupling reactions.[65,66] Up-to-date, the graphene with a well-defined molecular structure can only be prepared through this bottom-up approach. This chemically synthesized graphene is usually called "nanographene"; because the sizes of graphene sheets are limited to the nanometre scale by their low solubility. The well-defined structure of nanographene provides it with a controllable energy level, showing considerable importance in fundamental research on graphene based solar cells.[65–67]

2.2 GBMs with high specific surface areas

GBMs with high specific surface areas (SSAs) are widely used in supercapacitors and lithium ion batteries.[34,68] Graphene is one of the highest SSA materials, while the SSA of bulk graphite is quite low. However, the SSAs of GBMs are usually much lower than that of a single-layer graphene because of the π-stacking of graphene sheets.[69] Up-to-date, four strategies have been applied

Yiqing Sun

Yiqing Sun received her B.E. from the Department of Polymer Science and Engineering at Beijing University of Chemical Technology in 2009, and became a PhD candidate under the supervision of Prof. Gaoquan Shi in the Department of chemistry at Tsinghua University. Her research interests focus on graphene based materials.

Qiong Wu

Qiong Wu received his B.E. from the Department of Chemical Engineering at Tsinghua University in 2009. He is currently a M.S. candidate in Prof. Gaoquan Shi's laboratory at the Department of Chemistry of the same university. His research interests are clean energy materials based on conducting polymers and graphene.

Gaoquan Shi

Professor Gaoquan Shi received his BS degree (1985) and PhD degree (1992) in the Department of Chemistry at Nanjing University. Then he joined Nanjing University and was promoted to full professor in 1995. In 2000, he moved to Tsinghua University. His research interests are focused on synthesis and application of conducting polymers and graphene. He achieved 2nd place in the Natural Science of China and the Youth knowledge innovation competition of the Chinese Chemical Society and BASF Company in 2004.

to increase the porosities or SSAs of GBMs. First, rapid expanding is an effective technique for exfoliating stacked graphene sheets.[70–73] For example, high temperature treatment can reduce graphene oxide to r-GO and spontaneously generate a tremendous amount of gaseous species. In this process, the inner stress caused by gas release rapidly expanded r-GO sheets to single or few layers, yielding a highly porous spongy powder with a SSA up to 1500 $m^2 g^{-1}$.[70] The second strategy is stacking small graphene sheets into a porous structure. Direct reducing of a dilute graphene oxide dispersion leads to the formation of powdery r-GO particles. The particles have aggregated graphene sheets as cores and a number of extending individual graphene sheets as shells. This structure provides the material with a high SSA of 705 $m^2 g^{-1}$.[7] Interestingly, if a concentrated graphene oxide dispersion (*e.g.*, 2 mg mL^{-1}) was used, the r-GO sheets can be assembled into a three-dimensional network to form a hydrogel.[74] The regional π–π stacking of graphene sheets resulted in the formation of cross-linking cites and few-layer graphene sheets acted as the pore walls of the 3D network. Third, porous GBMs can be fabricated *via* template guided assembling of graphene sheets by using colloids, ice-crystals or polystyrene beads as the template.[75–77] Fourth, blending graphene sheets with other nanoparticles as "spacers" also can prevent graphene aggregation from forming composites with high SSAs.[69]

2.3 Thin films of GBMs

The window electrode of a solar cell is usually made of a transparent conductive film coated on a transparent substrate. Large area CVD graphene films have high transmittances and conductivities.[51,52] As initially deposited on metal foils, these films can be transferred to transparent glass or polymer substrates after etching away their metal supports.[53] An industrial applicable "roll-to-roll" technique for large area and continuous fabrication of transparent CVD graphene electrodes has also been developed.[78] On the other hand, small chemically converted graphene (CCG) sheets prepared through various wet chemical routes can be assembled into large thin films.[9,19] For example, CCG sheets prepared from different precursors such as graphite and graphene oxide can be functionalized into dispersible derivatives.[56,57,79,80] Thus, they can be fabricated into large conductive and transparent films by spin-coating, dip-coating, printing, filtration, electrophoretic deposition, or Langmuir–Blodgett assembly.[61,81–85]

2.4 Graphene based composites

In graphene-based composites, graphene acts either as a functional component or a substrate for immobilizing the other components. The large SSA and the conductive robust structure of graphene often facilitate the charge transfer, redox reaction as well as enforce the mechanical strengths of resulting composites. Therefore, anchoring redox active materials, electro- or photocatalysts on graphene will improve the performances of the resulting composites for water splitting and/or in energy storage and conversion devices.[10,38,43,86–88] For example, blending conjugated polymers or TiO_2 nanoparticles with graphene will promote their charge separation and transportation in photovoltaic and dye-sensitized solar cells.[87,89] Moreover, the aggregation of graphene sheets can be partly prevented by sandwiching the other nanomaterials, yielding highly porous composites attractive for fabricating high performance supercapacitors and fuel cells.[69] Recently, we have reviewed the preparation and applications of various graphene-based composite materials in detail.[90] Thus, herein, we briefly describe two general strategies of preparing GBMs as new energy materials: *in situ* reaction and blending.

Many graphene based composites with conducting polymers or inorganic nanoparticles were prepared *via in situ* chemical or electrochemical reactions.[91–94] In chemical syntheses, positively charged metal ions (*e.g.* Mn^{2+}) or monomer molecules (*e.g.* aniline hydrochloride) were preferred to adsorb on the negatively charged CCG *via* electrostatic and/or π–π stacking interactions.[91,92] Therefore, mineralization or polymerization occurred preferentially on CCG sheets to form the corresponding composite materials. Negatively charged ions, such as $PtCl_4^{2-}$, can also be reduced to metal nanoparticles on graphene sheets.[69] Besides, if graphene is a reactant (*e.g.* reducing MnO_4^- by graphene), the reaction is self-limited on the surface of graphene sheets.[95] In electrochemical processes, graphene sheets were deposited on a supporting electrode from the electrolyte containing functionalized soluble graphene.[94] The as-deposited graphene sheets acted as "nanoelectrodes" with high conductivity and SSA for successive depositing of the other nanomaterials. Besides, the traditional electrode can be replaced by a porous GBM for direct electrosynthesizing of the graphene based composite.[96]

Blending is one of the most convenient routes to graphene based composites. Chemically modified graphene sheets are usually soluble or dispersible in water or various organic solvents.[56,57,79,80] Thus, they can form composites by one-step solution-blending with organic molecules, polymers or inorganic nanostructures.[10,13,30,97] On the other hand, the large conjugated basal plane of graphene provides an ideal platform for assembling aromatic organic molecules and conducting polymers through π–π stacking.[13,97] Furthermore, graphene can be easily functionalized to either positively or negatively charged derivatives.[80,98] Thus, they can form composites with other charged components *via* direct blending or layer-by-layer assembly.[10,98] Based on these techniques, graphene composites with various functional materials including conducting polymers,[10,38,89] nanostructured metals,[30] metal oxides,[86] and other carbon nanomaterials[98,99] have been successfully prepared.

3. Applications of GBMs in energy related systems

3.1 Supercapacitors

Supercapacitors are a class of electrochemical devices for storing and releasing energies rapidly and reversibly.[22,100] A high-performance supercapacitor should have high energy density (1∼10 Wh kg^{-1}, determined by its capacitance and voltage), power density (10^3∼10^5 W kg^{-1}, determined by its voltage and internal resistance) and ultra-long cycling life (>100 000 cycles). Thus, supercapacitors act as perfect complements for batteries or fuel cells, and their co-operations are considered to be promising power supplies for versatile applications such as environmentally friendly automobiles, artificial organs, high-performance

portable electronics, *etc*. Supercapacitors can be simply classified by their storage mechanisms into two groups: electrical double-layer capacitors (EDLCs) and pseudo-capacitors.[101] Actually, these two storage mechanisms often occur simultaneously, and are inseparable in real systems. For the convenience of studies however, the electrode materials are divided into both groups according to their dominant storage mechanism.

3.1.1 Electrical double layer capacitors (EDLCs). The capacitance of an EDLC is generated by electrostatic charge accumulation at the electrode/electrolyte interfaces, and is usually proportional to the effective SSA of electrode material.[100] Details about the energy storage mechanism of EDLCs can be found in previous publications.[100,102,103] In order to obtain a high double-layer capacitance, the SSAs of electrode materials should be maximized. Furthermore, the pore structures and surface properties of the electrodes should be controlled to ensure the availability of their surface areas for forming electrical double-layers. Besides high SSA, several other parameters are of equivalent importance for supercapacitor: high power performance requires low resistance of the electrodes and electrolyte, and a long cycling life demands high electrochemical, thermal and mechanical stability of the electrode materials. Moreover, safety, environmental benignity and cost-effectiveness should also be considered. In view of the requirements described above, porous carbon materials are most promising for EDLCs due to their good supercapacitor performances, various existing forms, easy processibility and abundance.[103–106] Porous carbons were usually prepared by three strategies: activation, template guided synthesis, and self-assembly. Table 1 compares the SSAs and mass-specific capacitances (C_m) of EDLCs based on carbon materials prepared through different strategies according to literature results.[25,68,103,104] As shown in Table 1, activation usually results in the formation of carbon materials with high SSAs, while having uncontrollable pore structures and oxygenated functionalities. Thus, the inaccessible pores, unstable oxygenated groups and high inherent resistance of activated carbon materials usually limit their performance. The template guided synthesis method, using a hard (*e.g.* zeolite) or soft (*e.g.* polymers) template, is effective for preparing porous carbons or carbon aerogels with controllable pore structures. These porous carbons exhibited good performances in supercapacitors. However, the hard template technique is limited by its high cost and elaborate procedure. On the other hand, carbon aerogels are cheap, while they suffer from low specific capacitance. In comparison, the self-assembly of carbon nanotube (CNT) or graphene into porous carbon nanomaterials is the most effective and convenient strategy.

Table 1 Comparison of the EDLCs based on different carbon materials.[25,68,103,104]

Carbon based EDLC materials	SSA (m^2 g^{-1})	C_m (F g^{-1})
Activated carbon	1000∼3500	< 200
Activated carbon fiber	1000∼3000	120∼370
Templated carbon	500∼3000	100∼350
Carbon aerogel	400∼1000	100∼125
Carbon nanotube	120∼500	15∼135
GBMs	<1500	14∼264

According to Table 1, the C_m of graphene is higher than that of CNT in most cases, and the potential of graphene is more attractive because of the following three factors: (1) graphene has a higher theoretical SSA and can be prepared on a large scale at a low cost;[7] (2) graphene is inherently non-porous, and all pores in a GBM can be regulated by controlling its microstructure;[38,74] (3) graphene has an excellent electron mobility. For example, an EDLC based on vertically aligned graphene sheets showed an ultrafast frequency response, which is comparable to that of an aluminium electrolyte capacitor.[85] Generally, graphene based EDLC materials can be prepared through four strategies as compared in Table 2,[7,37,38,70,74,86–95] and will be discussed in the following sections.

3.1.1.1 Chemical or thermal reduction of graphene oxide in its dispersions. As reported by Ruoff and co-workers, chemically reducing graphene oxide in its aqueous dispersion resulted in the formation of "graphene-based nanosheets", which are nanoparticles consisting of partially aggregated r-GO sheets.[107] Graphene sheets were randomly stacked with individual graphene sheets extending from the outer surfaces of these nanoparticles (Fig. 1a). [7] Therefore, both sides of these extended graphene sheets are partly exposed to electrolyte and available for forming electrical double-layers. Besides, porous powdery r-GO can also be obtained by thermally reducing graphene oxide in an organic solvent with a high boiling point.[108,109] This r-GO material was tested to have a C_m comparable to those of most carbon materials.

3.1.1.2 Reducing powdery graphene oxide into porous GBMs. Thermal reduction of graphene oxide powder at a high temperature (1050 °C) rapidly generated a large amount of gaseous species and exfoliated r-GO sheets into a porous structure with high SSA.[70,71] However, this material exhibited a moderate C_m (117 F g^{-1}), mainly due to the large proportion of its inaccessible micropores.[71] Two research groups modified the thermal exfoliation process and yielded mesoporous graphene and porous functionalized graphene with C_ms of 150 and 233 F g^{-1}, respectively.[110,111] In order to promote the thermo-induced exfoliation, high-vacuum[72] or microwave treatment [73] has been applied as an assistant technique to generate a GBM with a high C_m of 264 or 191 F g^{-1}. Besides, exposing graphene oxide powder to hydrazine vapor is also an alternative strategy to reduce graphene oxide powder into a porous material.[112]

3.1.1.3 Assembling graphene sheets into GBMs with ordered 2D or 3D microstructures. Recently, we prepared a self-assembled graphene hydrogel (SGH) *via* a one-step hydrothermal reduction.[74] This SGH has a 3D network consisting of ultrathin graphene walls and cross-linking sites formed by regional π–π stacking of graphene sheets (Fig. 1b). This unique structure endows the SGH with high mechanical strength, conductivity as well as high C_m. More importantly, this method can be extended to fabricate composite materials with other carbon nanomaterials or electroactive species for fabricating high performance EDLCs or pseudo-capacitors. Recently, it was also reported that graphene sheets could be assembled into 3D porous macrostructures with the assistance of either noble metal nanoparticles[113] or DNA molecules.[114] In comparison, assembling

Table 2 Comparison of the performances of GBMs prepared by different methods for EDLCs

Graphene based EDLC materials	SSA (m^2 g^{-1})[a]	C_m (F g^{-1}) Aqueous	C_m (F g^{-1}) Organic	Rate capability[b]	Cycle life[b]	Ref.
r-GO, chemical reduction in an aqueous dispersion	705	135	99	0.4 V s^{-1} (96%)	—	7
r-GO, thermal reduction in an organic dispersion	—	—	120	0.04 V s^{-1} (85%)	—	108
r-GO, microwave assisted reduction in an organic dispersion	—	100	—	—	—	109
r-GO, thermal reduction (dry)	925	117	—	1 V s^{-1} (85%)	—	71
	524	150	—	1 A g^{-1} (93%)	500 (100%)	110
	404	233	73	0.1 V s^{-1} (43%)	—	111
r-GO, vacuum assisted thermal reduction (dry)	368 (1000[c])	264	122	0.8 V s^{-1} (65%)	100 (97%)	72
r-GO, microwave assisted thermal reduction (dry)	463	191	—	0.6 A g^{-1} (91%)	—	73
r-GO, hydrazine vapor reduction	320	205	—	—	1200 (90%)	112
Self-assembled graphene hydrogel	—	175	—	0.02 V s^{-1} (87%)	—	74
Ultrathin graphene film (25∼100 nm thick)	—	111∼99	—	—	—	115
Assembled graphene film	—	80	—	—	1000 (98%)	116
Graphene/carbon onion composite	417	143	—	10 A g^{-1} (55%)	5000 (100%)	[d]
Graphene/carbon black composite	586	175	—	0.5 V s^{-1} (67%)	6000 (91%)	99
Layer-by-layer assembled graphene/CNT composite	—	124	—	1 V s^{-1} (97%)	—	98
Graphene/CNT sandwich	312	385	—	—	2000 (−20%)	117

[a] According to BET method, except for those noted. [b] The percentage in brackets represents the capacitance retention in the given conditions. [c] Measured by methylene blue adsorption. [d] Unpublished.

graphene sheets into 2D films is not appropriate for fabricating EDLCs electrodes. For instance, filtration of the dispersion of graphene sheets usually induces the formation of a compact film because of the π–π stacking interaction. Although the obtained thin film has good mechanical strength, high conductivity and flexibility, their SSA is quite low.[16] An ultrathin film (*e.g.*, 25 nm) showed a moderate C_m of 111 F g^{-1}, and this value was further decreased by increasing its thickness.[115] Assembling graphene sheets into a free-standing film with a controlled microstructure seems to be an effective strategy for increasing its porosity, but the C_m of the assembled film is still unsatisfactory.[116]

3.1.1.4 Separating graphene sheets with other nanomaterials. Graphene based films failed to maintain the high SSAs of their individual sheets; therefore, various "spacer" materials were introduced to overcome this problem.[69,99,117] Recently, we assembled nanodiamond particles between graphene oxide sheets *via* filtration. The high-temperature treatment of the graphene oxide/nanodiamond composite reduced graphene oxide and converted diamond particles to porous carbon onions. The obtained r-GO/carbon onion composite film is flexible and has a mesoporous structure. Thus, it exhibited very high conductivity, large SSA and C_m. Moreover, carbon black (CB) nanoparticles were also used as the "spacers" of graphene sheets.[99] However, the C_m of the CB composite with single layer graphene is lower than that of the composite prepared from few layers graphene. This is probably due to the addition of a small amount of CB (*e.g.* 10 wt%) which efficiently isolated the aggregated graphene nanosheets, but failed to effectively separate the single-layer graphene sheets. In addition, *in situ* growth and LBL assembly have been used for preparing graphene/CNT composites.[98,117] In comparison, the C_m of *in situ* grown graphene/CNT

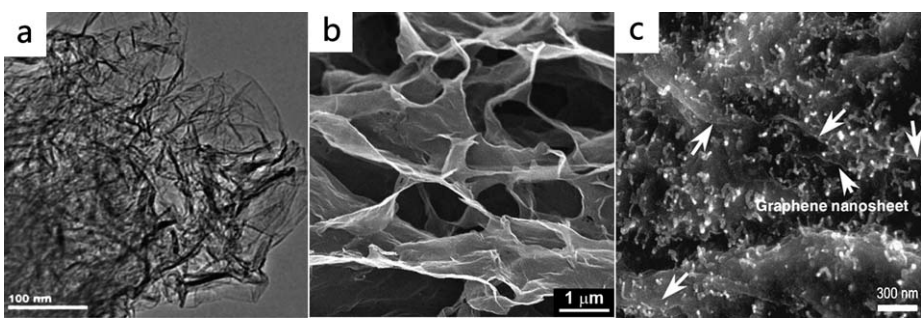

Fig. 1 (a) TEM image of graphene-based nanosheets, reproduced with permission from ref. 7 © 2008 American Chemical Society. (b) SEM image of a self-assembled graphene hydrogel, reproduced with permission from ref. 74 © 2010 American Chemical Society. (c) SEM image of a CNT/graphene composite, reproduced with permission from ref. 117 © 2010 Wiley-VCH.

composite was tested to be much higher than that of the LBL assembled counterpart. In the former composite, CNTs are vertically aligned on the graphene sheets with a sandwich structure (Fig. 1c) and graphene sheets are effectively separated by them. In the latter one, however, CNTs lie down on graphene sheets; thus, the regional aggregation of graphene sheets is unavoidable.

3.1.2 Pseudo-capacitors. Pseudo-capacitors store their energies *via* faradaic processes (redox or adsorption).[101] The adsorption pseudo-capacitances are mainly attributed to the surfaces of precious metals and their contributions are negligible in most practical systems; therefore, "pseudo-capacitance" and "redox capacitance" are usually the same. Compared with EDLCs, pseudo-capacitors have much larger C_ms, but usually exhibit lower working voltages and worse cycling stability.[25,100,101] In principle, any materials with fast and reversible redox properties can be used for fabricating pseudo-capacitors. For practical applications, however, they should be cheap and insoluble in electrolyte. Up-to-date, the most attractive materials for pseudo-capacitors are conducting polymers (*e.g.* polyaniline)[10,91,93,96] and cheap transition metal oxides or hydroxides (*e.g.* MnO_2 and $Ni(OH)_2$).[92,95,118] These electroactive materials have high theoretical C_ms and intrinsically fast and reversible redox reactions.[25] However, the applications of their pure materials are limited by following two factors. First, the low conductivities of neutral conducting polymers and oxides or hydroxides restrict fast electron transportations. As a result, large proportions of the materials are dead at high charging/discharging rates. Second, rapid redox reactions often occur at electrode surfaces. Thus, the inner parts of the materials are useless. To deal with both problems, anchoring nanostructured active materials onto carbon-based materials with high conductivities and SSAs is an effective approach.[119] Therefore, graphene is one of the most promising substrate materials for fabricating the electrodes of pseudo-capacitors. Table 3 compares the performances of several pseudo-capacitors based on graphene composites.[10,91–96,120]

3.1.2.1 Conducting polymer/graphene composite. Polyaniline (PANI) is the most widely used conducting polymer for fabricating pseudocapacitors. PANI has multiple redox states and good environmental stability. Furthermore, it can be cheaply and facilely fabricated into nanostructures.[121,122] However, PANI usually suffers from degradation induced by the volume changes during the repeated charging/discharging process.[100] In this case, the robust and flexible graphene sheets could sustain and buffer the volume changes of PANI, and the high conductivity of graphene would further decrease the resistance of the composites.

In situ polymerization of aniline in the presence of graphene-based nanosheets can produce PANI/graphene composites with a sandwich structure.[91] PANI was grown on the surface of a graphene-based nanosheet rather than in solution, probably due to the preferential adsorption of aniline molecules on the graphene sheets *via* electrostatic and π–π interactions. Although the starting material was slightly-aggregated graphene sheets rather than single-layer graphene, the resulting composite showed a very high C_m (1046 F g^{-1}), indicating the synergic effect of both components. In another paper, graphene oxide was used instead of graphene as the starting material, producing a graphene oxide/PANI nanofiber (PANI-NF) composite and was followed by reducing graphene oxide to r-GO.[93] This composite also showed high C_m and good rate-performance.

However, the polymerization of aniline can be successfully carried out only in a strong acidic medium (usually pH = 0), in which either graphene oxide or single-layer graphene will be severely aggregated. Therefore, it is difficult to prepare single-layer graphene/PANI composite materials by *in situ* polymerization. This problem can be overcome by using a self-assembly strategy. Chemically converted graphene (CCG) sheets are negatively charged and polyaninine nanofibers (PANI-NF) are positively charged.[56,123] Thus, both components can be self-assembled through electrostatic interaction into a uniform composite.[10] Under controlled conditions, CCG/PANI-NF composite could be stably dispersed in water and assembled to a flexible film *via* filtration. The obtained film showed good performance owing to its ordered layer structure (Fig. 2a); however, its C_m is lower than that of the powdery counterparts because of small SSA. Another route to flexible graphene/PANI composite film is the electrochemical polymerization of aniline directly on a porous graphene paper and the obtained composite paper also showed good electrochemical and mechanical properties.[96] Electrochemical co-deposition is another route to conducting a polymer/graphene composite. For example, sulfonated graphene (SG) sheets and polypyrrole (PPy) could be co-deposited into a porous composite film from the aqueous electrolyte containing SG and pyrrole monomer. The resulting SG/PPy composite film showed a C_m of 285 F g^{-1}.[94]

Table 3 Performance of several pseudo-capacitors based on graphene composites

Composites	Preparation method	C_m (F g^{-1})	Rate capability[a]	Cycle life[a]	Ref.
PANI/graphene-based nanosheet	*In situ*	1046	0.05 V s^{-1} (62%)	—	91
PANI-NF/graphene	*In situ*	480	1 A g^{-1} (44%)	1000 (70%)	93
PANI-NF/graphene composite film	Self-assembly	210	3 A g^{-1} (94%)	800 (79%)	10
PANI/graphene paper composite film	*In situ* electrochemical	233	—	1400 (−10%)	96
PPy/graphene	Electrochemical co-deposition	285	10 A g^{-1} (73%)	800 (92%)	94
MnO_2/graphene oxide	*In situ*	216	1 A g^{-1} (51%)	1000 (84%)	92
MnO_2/graphene-based nanosheet	Self-limiting reaction	310	0.5 V s^{-1} (74%)	15000 (95%)	95
$Ni(OH)_2$ nanoplate/graphene	*In situ*	935	45.7 A g^{-1} (71%)	2000 (~100%)	118
$Co(OH)_2$/graphene	*In situ*	972.5	—	—	120

[a] The percentage in brackets represents the capacitance retention in the given conditions.

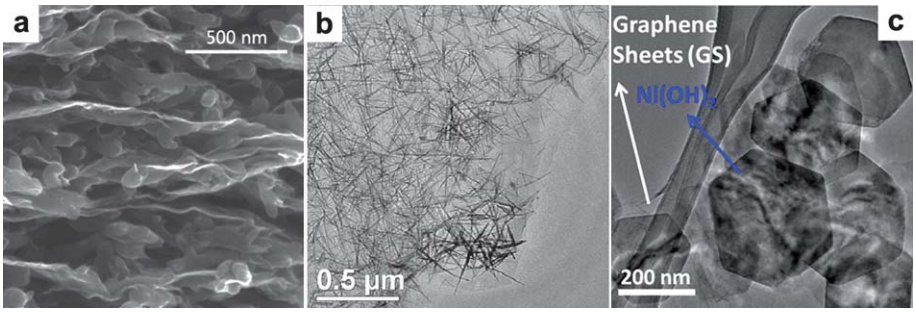

Fig. 2 (a) Cross-section SEM image of a PANI-NF/graphene composite film, reproduced with permission from ref. 10 © 2010 American Chemical Society. (b) TEM image of a MnO_2 nanoneedle/graphene oxide composite, reproduced with permission from ref. 92 © 2010 American Chemical Society. (c) TEM image of a $Ni(OH)_2$ nanosheet/graphene composite, reproduced with permission from ref. 118 © 2010 American Chemical Society.

3.1.2.2 Metal compound/graphene composites. Among metal compounds, MnO_2 is promising for pseudo-capacitors because of the rapid redox reaction at its particle surfaces, low-cost, stable, and environmental friendliness. A MnO_2 nanoneedle/graphene oxide composite has been successfully prepared.[92] Although the composite has a uniform morphology (Fig. 2b), its C_m is moderate and its rate performance is unsatisfactory. The loss of C_m at a high discharging rate was attributed to the decrease of available pores of the composite because of its low conductivity. In comparison, as conductive graphene-based nanosheets were used as the starting material, the resulting composite exhibited high C_m, good rate performance and long cycling life.[95]

Dai and co-workers reported the *in situ* growth of single-crystalline $Ni(OH)_2$ nanoplates on graphene sheets (Fig. 2c).[118] As a 2D conductive substrate, graphene is a unique component for preparing its composites with 2D $Ni(OH)_2$ nanoplates. The synergistic effect of both components rendered the composites with an extraordinary high C_m of 935 F g^{-1}. Similarly, a $Co(OH)_2$/graphene composite was prepared and exhibited a even higher C_m.[120]

3.2 Lithium ion batteries

Lithium ion battery (LIB) is considered to be one of the most useful batteries in portable electronics due to its high voltage, high energy density, long cycling life and good environment compatibility.[23,26] However, with the development of electronic devices, especially in electric vehicles, there are continuous demands for batteries with higher power and energy densities, and longer cycling life. On the other hand, LIB is recognized as a rock-chair battery with Li^+ insertion/excitation in the two electrodes during the charging/discharging processes.[26] Thus, the performance of a LIB strongly depends on the structures and properties of its electrodes. Graphite is the commercialized anode because of its good life cycle performance and high coulombic efficiency.[26,124] However the specific capacity (C_s) of graphite is limited to 372 mA h g^{-1} by forming an intercalation compound of LiC_6.

In order to improve the performance of LIBs, anode materials with specific capacities (C_s's) higher than that of graphite are required. A variety of carbon nanomaterials such as carbon nanofibers,[125,126] carbon nanotubes[127,128] and mesoporous carbons[129,130] have been explored for this purpose. The diffusion distances of lithium ions in the nanostructured carbons are short, leading to improved rate performances.[23] Apart from carbon nanomaterials, silicon, metals and oxides were also studied for replacing graphite as the anode materials of LIBs. The C_s's of these materials are much higher than that of graphite. However, one of the main drawbacks of these materials is their huge volume variations during the processes of lithium insertion/extraction.[46,47,131] The volume changes of the electrodes can cause the pulverization of the whole electrode. Another problem is that most metal oxides have poor electrical conductivities. Thus, the blending of carbon nanomaterials into these inorganic materials is considered to be the most efficient method to overcome both problems described above.[47] On the basis of these considerations, graphene and its composites should have a great potential as the anode materials of LIBs.[46]

3.2.1 Graphene anodes. Compared with graphite, graphene has a huge SSA of 2600 m^2 g^{-1}, and more edge sites for anchoring other electroactive materials.[132,133] Thus, it possesses a much larger theoretical C_s, and this assumption has been confirmed by different experiments.[11,75,133–136] The Li storage of graphene nanosheets was first investigated by Kudo and co-workers.[11] The C_s of the graphene sheets prepared by the reduction of graphene oxide was found to be 540 mA h g^{-1}, which is much larger than that of graphite. Furthermore, when carbon nanotubes or fullerene were incorporated into graphene, the C_s of the corresponding composite increased to 730 or 784 mA h g^{-1} as shown in Fig. 3. It was found that the C_s s of these composites increased with the contents of their interlayer spacing species. Thus, the researchers believed that the mechanism of Li storage in graphene was different from that in graphite. Park *et al.* think that lithium can be adsorbed on both sides of a single graphene nanosheet with a theoretical C_s of 744 mA h g^{-1} by the formation of Li_2C_6, similar to that of hard carbons.[136] However, the C_s of tiny graphene sheets with diameters around 0.7 nm was calculated to be 1488 mA h g^{-1} by forming Li_4C_6.[137] Kostecki *et al.* indicated that the interaction of lithium with few-layers graphene resembled that of bulk graphite, which seems to be different in the case of single-layer graphene.[138] The edge effect on the characteristics of Li diffusion in graphene was theoretically investigated by Uthaisar *et al.* using the density functional theory.[139] It was clearly demonstrated that narrower graphene

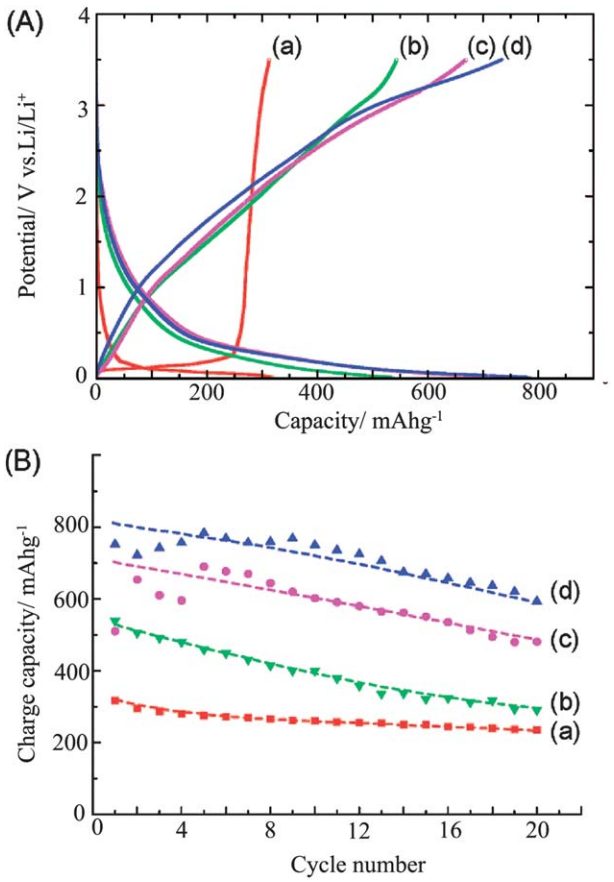

Fig. 3 (A) Charge/discharge profiles and (B) charge/discharge cycle performances of (a) graphite, (b) graphene, (c) graphene + CNT, and (d) graphene + C_{60} at a current density of 0.05 A g^{-1}, reproduced with permission from ref. 11 © 2008 American Chemical Society.

nanosheets should possess faster discharge performance, mainly due to their decreased energy barriers and diffusion lengths. Jiao and co-workers studied the lithium storage in highly disordered graphene nanosheets. They concluded that the greatly enhanced C_s of graphene is mainly ascribed to its additional reversible storage sites such as edges and other defects.[133] On the basis of the facts described above, the mechanism of lithium storage in graphene is still an ongoing debate. The Li interaction/extraction processes in graphene materials need to be further clarified in the future.

Graphene powders produced by different methods have been widely explored for the applications as anode materials of LIBs.[11,136] Kudo *et al.* prepared a LIB anode from few-layers graphene nanosheets (10∼20 layers) by the chemical reduction of graphite oxide, and a C_s of 540 mA h g^{-1} was obtained.[11] An improved reversible C_s of 650 mA h g^{-1} was achieved by using the chemically synthesized graphene sheets (2∼3 layers) due to their loose agglomeration and less-layers stacking.[136] After a long-term cycling over 100 cycles, its C_s decreased to 460 mA h g^{-1}.

Compared to the graphene prepared by chemical reduction, thermal exfoliated graphene has a higher C_s. The graphene made from graphite by oxidation, rapid expansion and ultrasonic treatment was tested to have an initial C_s as high as 1233 mA h g^{-1} and a reversible C_s of 672 mA h g^{-1}.[135] Graphene nanosheets prepared from the rapid thermal expansion of graphite oxide in nitrogen atmosphere were reported to have a C_s of 1264 mA h g^{-1} at the first cycle and it decreased to 848 mA h g^{-1} after 40 cycles.[136]

Considering the flexible, self-supporting and electrically conductive properties of graphene films, they have potential applications in flexible energy storage devices. The lithium storage in graphene films was firstly investigated by Wallace and co-workers.[140] The discharge C_s of a graphene film was measured to be 680 mA h g^{-1} during the first discharge process and it decreased to only 84 mA h g^{-1} at the second cycle. Nguyen *et al.* discussed the rate performance of the graphene film. The C_s of the graphene film was increased from 84 to 214 mA h g^{-1} as the discharge current density decreased from 50 to 10 mA g^{-1}. It is suggested that the layered structure of graphene film might create barriers to Li ion diffusion.[141] Song *et al.* prepared hollow graphene oxide spheres (HGOS) *via* a water-in-oil (W/O) emulsion technique without the assistance of a surfactant (Fig. 4). After thermal reduction, the resulting hollow graphene spheres exhibited a high C_s of 485 mA h g^{-1} and an improved rate performance because of its hollow structure and porous thin graphene shells. [75]

Although the C_s's graphene anodes are much larger than that of graphite, there are several issues which need to be addressed for their practical applications.[132] One of the disadvantages of these anodes is their high irreversible capacities in the first cycles. This is mainly due to the irreversible reaction between lithium and the functional groups of graphene sheets and the formation of a solid electrolyte interface (SEI). These problems can be partly solved by surface modification of graphene sheets.[135,142] Another problem is the poor rate performances of graphene anodes.[136] However, the most serious problem of graphene anodes is that their galvanostatic discharge curves do not give potential plateaus. This phenomenon indicates the LIBs with graphene anodes cannot provide stable potential outputs, which will hold back its practical applications.

3.2.2 Graphene composites as anode materials. Many metals and their oxides are also promising anode materials of LIBs because of their huge theoretical lithium ion storage capacities.[46,47,143–145] Blending these materials with graphene to form composites can improve their performance. Examples are the composites of graphene and metal or oxide nanoparticles. Several metals such as Sn and Sb can be used as the anodes of LIBs, because they can reversibly form alloys with lithium. For example, the reaction between lithium and Sn can be described as follows:

$$4.4Li^+ + Sn + 4.4e^- \leftrightarrow Li_{4.4}Sn$$

The theoretical reversible C_s of Sn is about 994 mA h g^{-1}, which is much larger than that of graphite (372 mA h g^{-1}).[144] However, Sn nanoparticles tend to aggregate during the cycling process, causing a rapid decrease of its capacity. This problem can be partially resolved by depositing Sn nanoparticles on graphene sheets to form a 3D nanostructure.[144] The resulting graphene/Sn composite showed a discharge C_s of 1250 mA h g^{-1} in the first cycle, 810 mA h g^{-1} in the second cycle and 508 mA h

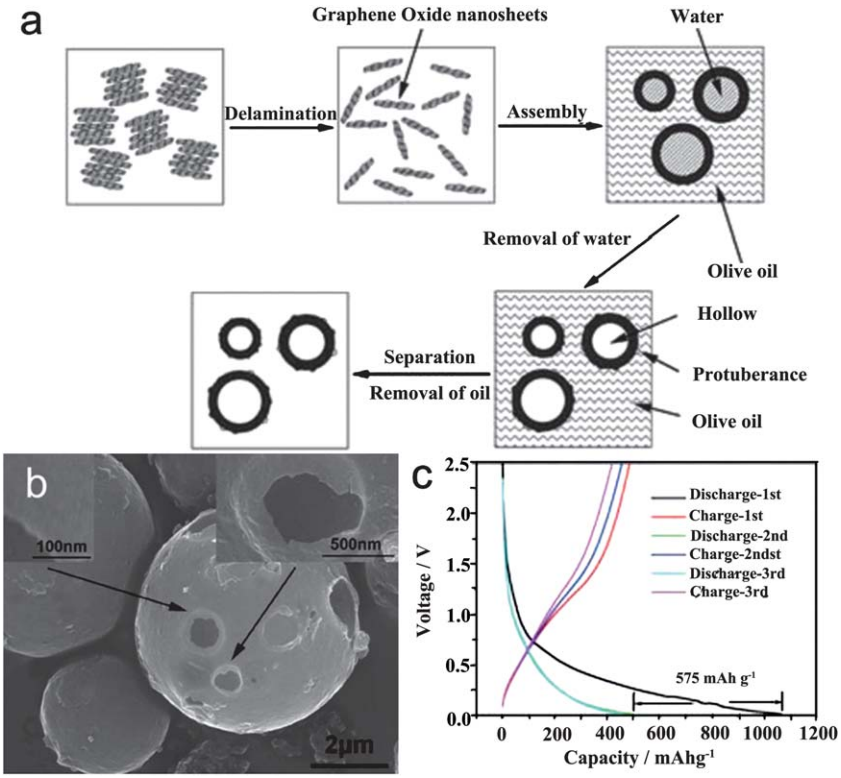

Fig. 4 (a) Schematic illustration of the HGOSs preparation process. (b) SEM images of HGOSs. (c) The first three charge/discharge curves of HGOSs, reproduced from ref. 75 with permission, © 2010 Royal Society of Chemistry.

g^{-1} after 100 cycles. The performance of the composite is much better than that of each component. Theoretical analysis by the first principle calculations indicated that lithium can be stably stored on both sides of graphene sheets (Li_2C_6, 744 mA h g^{-1}).

Silicon is one of the most attractive electrode materials, because it possesses the highest theoretical energy density among common simple substances.[146] Furthermore, it is cheap and easy to handle. However, the large volume change (up to 270% for the $Li_{3.75}Si$ phase) and losing electrical contact during lithium insertion/extraction of Si electrode usually result in the fading of its capacity.[147] Thus, the lithium storage property of graphene/Si composite was studied. Dou *et al.* compared the performance of graphene, silicon nanoparticle, and Si/graphene composite electrodes.[147] The C_s of pristine graphene decreased from 1274 to 204 mA h g^{-1} after 10 cycles. The anode of silicon nanoparticles showed an initial discharge C_s of 3027 mA h g^{-1}, and dropped to 346 mA h g^{-1} after 30 cycles. In comparison, the composite exhibited a much better performance; it still kept a high C_s of 1168 mA h g^{-1} after 30 cycles. Electrochemical impedance spectroscopy was also used to study the electrochemical properties of the composite. It was found that the resistance of graphene was lower than that of silicon nanoparticles, implying the enhanced conductivity of the composite. Moreover, the authors believed that the high SSA and porous structure of the composite also facilitated the penetration of the electrolyte as well as buffered the volume change of the electrode. A silicon/graphene composite with a 3D graphitic network structure was prepared. In this composite, silicon nanoparticles were uniformly dispersed on graphene sheets and the 3D graphitic network was formed by regional stacking of graphene sheets at their reconstituted domains.[146] The C_s of the composite was measured to be above 2200 mA h g^{-1} after 50 cycles and 1500 mA h g^{-1} after 200 cycles. The regional reconstitution of graphene sheets into graphite forms a continuous and highly conductive 3D network, which resulted in improving the performance of the electrode. The 3D network not only served as a structural scaffold to anchor graphene sheets for sandwiching and trapping Si nanoparticles, but also enhanced the electrical conductivity of the composite.

Other options for the anode materials of LIBs are transition metal oxides, such as Co_3O_4, Fe_2O_3, TiO_2, SnO_2, *etc.*[144] Graphene has also been blended with these oxides to improve their performances.[46,47,131,143,148–152] For example, SnO_2 nanoparticles were assembled onto the graphene sheets dispersed in ethylene glycol.[46] The graphene sheets formed a nanoporous structure in which SnO_2 nanoparticles were loosely packed. The obtained composite exhibited a high C_s of 810 mA h g^{-1} in the first cycle and 570 mA h g^{-1} after 30 cycles. However, the electrodes of bare SnO_2 showed a C_s of only 550 mA h g^{-1} in the first cycle and this value dropped to 60 mA h g^{-1} after 15 cycles (Fig. 5). It is believed that the existence of the graphene component can confine the volume change of the electrode in the charge/discharge process and the porous structure of the electrode can further buffer its volume change (Fig. 5c). Wang *et al.* prepared a SnO_2/graphene composite by reducing graphene oxide in the presence of $SnCl_2$ at a temperature of 120 °C.[131] This composite exhibited a discharge C_s of 1420 mA h g^{-1} in the first cycle and a reversible C_s of 765 mA h g^{-1}. Aksay *et al.* also synthesized a SnO_2/graphene composite with a well-defined nanostructure by

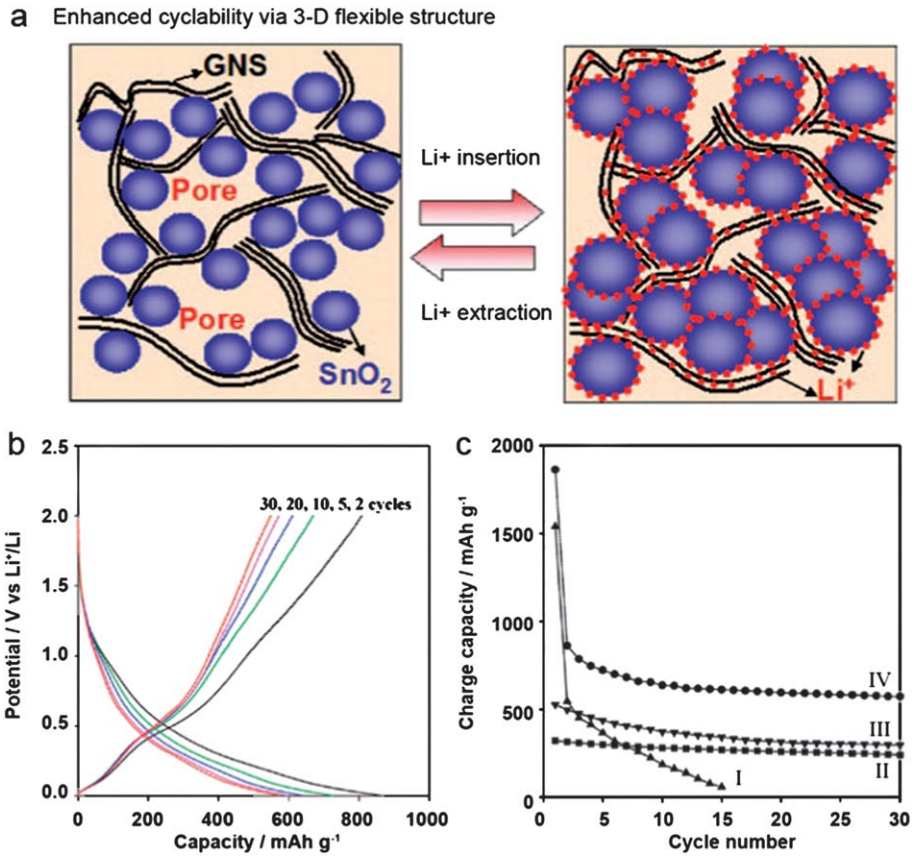

Fig. 5 (a) Schematic illustration of the synthesis and the structure of SnO2/GNS. (b) Charge/discharge curves of a SnO_2/graphene composite. (c) Cyclic performances of bare SnO_2 nanoparticles (I), graphite (II), graphene (III), and (d) SnO_2/graphene composite (IV), reproduced with permission from ref. 46 © 2009 American Chemical Society.

the assistance of a surfactant (Fig., 6a).[148] The steady C_s of the composite was tested to be 625 mA h g^{-1} after 10 cycles, and this value did not show a significant fade over 100 cycles.

TiO_2 is one of the attractive anode materials for LIBs because of its abundance, low cost and environmental friendliness.[47] In addition, TiO_2 is also structurally stable during the process of insertion and extraction of lithium. However, its conductivity is low. The addition of graphene can partially overcome this problem. Liu *et al.* prepared a TiO_2/graphene hybrid nanostructure by *in situ* growing TiO_2 nanocrystals on graphene sheets (Fig. 6b, c).[47] The composite has a much higher conductivity than that of TiO_2. As a result, it showed an enhanced lithium insertion and extraction kinetics compared with bare TiO_2 especially at high charge/discharge rates. Spinel $Li_4Ti_5O_{12}$ is also a promising anode material for LIBs due to its well-known zero-strain merits and the absence of forming surface lithium.[23,152,153] Zhu *et al.* prepared a nanostructured $Li_4Ti_5O_{12}$/graphene composite by electrospinning (Fig. 6d).[152] The blending of graphene can improve the electron mobility of the composite, which is identified by its better rate performance than that of pure $Li_4Ti_5O_{12}$.

Co_3O_4 is another anode material with high theoretical capacity (890 mA h g^{-1}).[151] However, similar to SnO_2, it also has a large volume change during a charge/discharge process. A composite of Co_3O_4 nanoparticles and graphene was prepared by hydrolysis Co^{2+} salt on graphene sheets in an alkaline aqueous medium

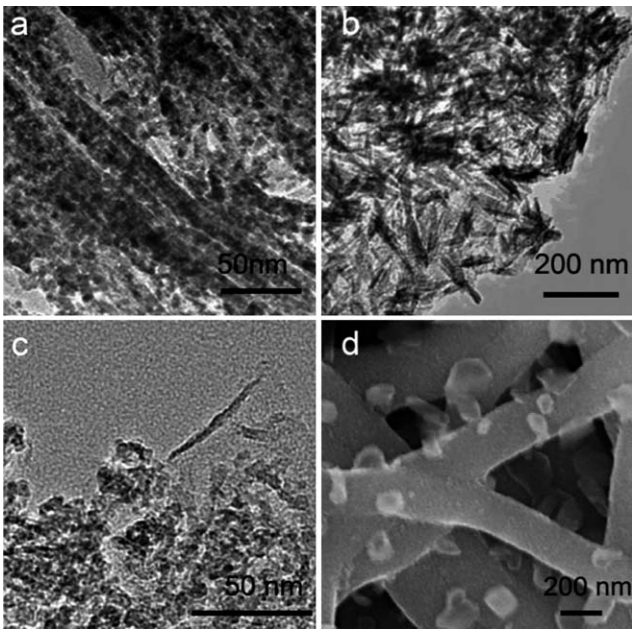

Fig. 6 (a) TEM image of a SnO_2/graphene composite, reproduced with permission from ref. 148 © 2010 American Chemical Society. (b, c) TEM images of (b) rutile and (c) anatase TiO_2 nanoparticles lying on graphene sheets, reproduced with permission from ref. 47 © 2009 American Chemical Society. (d) The nanostructure of a graphene doped $Li_4Ti_5O_{12}$, reproduced with permission from ref. 152 © 2008 Elsevier B.V.

and the resulting $Co(OH)_2$/graphene composite was calcinated at 450 °C.[151] The C_s of this composite was tested to be 800 mA h g^{-1} in the first cycle, and increased to 935 mA h g^{-1} after 30 cycles. Compared to the composite, the reversible C_s of graphene (or bare Co_3O_4) decreased from 955 to 638 mA h g^{-1} (or from 817 to 184 mA h g^{-1}) within 30 cycles. Müllen's group prepared the composites of Co_3O_4 nanoparticles and graphene by the calcination of cobalt phthalocyanine/graphene composites.[150] The cobalt phthalocyanine anchored to graphene sheets through π–π interaction. This technique prevented the molecular aggregation of the planar phthalocyanine, the precursor of Co_3O_4, and resulted in the formation of a uniform composite. This composite has a reversible C_s of 760 mA h g^{-1} after 20 cycles, which is higher than that of graphene or Co_3O_4. Furthermore, it showed an improved rate performance. Co_3O_4/graphene composite can also be prepared by assembling positively charged Co_3O_4 nanoparticles on negatively charged graphene oxide sheets, and graphene oxide was successively reduced to graphene. This electrostatic self-assembly strategy resulted in sandwiching the nanoparticles between graphene layers. In this composite, graphene sheets provided a conductive network and also prevented the aggregation of the nanoparticles.[150] As a result, a very high reversible C_s of 1000 mA h g^{-1} (after 130 cycles) was observed from this composite.

3.2.3 Graphene composites as cathode materials. Due to its low cost, environmental compatibility, good cycling stability and high theoretical specific capacity of 170 mA h g^{-1}, $LiFePO_4$ has been widely explored as a cathode material for LIB.[154,155] However, the practical application of $LiFePO_4$ has been limited by its low conductivity. The addition of a carbon nanomaterial such as carbon black[156] or carbon nanotube[157] is one of the most effective methods to improve the conductivity of $LiFeO_4$. Recently, graphene has also been used for this purpose. Zhang *et al.* prepared a $LiFePO_4$/graphene composite by the co-precipitation of both components.[158] The composite with only 1.5 wt% graphene exhibited a discharge specific capacity of 160 mA h g^{-1} at 0.2 C and 110 mA h g^{-1} at 10 C. A similar composite was also prepared through a hydrothermal route.[159] Yang and co-workers compared $LiFePO_4$/graphene and $LiFeO_4$/carbon black composites as the cathodes of LIBs.[160] The results showed that the performance of a $LiFePO_4$/graphene composite with only 2 wt% graphene was better than that of the $LiFeO_4$/carbon black composite with 20 wt% of carbon black. This is mainly due to $LiFePO_4$/graphene following a "plane-to-point" conducting mode while $LiFeO_4$/carbon black follows a "point-to-point" mode. As a result, the 2D graphene sheets are more likely to form a conducting network than carbon black.

3.3 Electrocatalysts for fuel cells

Fuel cell is one of energy conversion devices, which generates energy by oxidizing a fuel catalyzed by the catalysts immobilized on electrodes.[161] Fuel cells, especially the low temperature fuel cells, have a important application as portable power sources for distributing or remote generating of electrical energy.[23] Low temperature fuel cell usually works at the temperatures below 200 °C, which can electrochemically convert hydrogen into water or methanol–ethanol into water and carbon dioxide.[162] Therefore, the performance of fuel cells mainly depends on their electrodes. Platinum and its alloys are the most efficient catalysts used in fuel cells.[23,162,163] However, the high price of platinum limits its practical applications. Immobilizing Pt nanoparticles on a substrate with high SSA is the most widely used technique for improving the activity and efficiency of Pt catalyst. Graphene is an ideal catalyst support, mainly due to its high electrical conductivity, excellent mechanical properties, high SSA, unique graphitic basal plane structure and potential low manufacturing cost. A great deal of effort has also been devoted to seeking alternative materials with high catalytic activities and low prices for replacing Pt. Among them, nitrogen doped carbon materials such as nitrogen doped carbon nanotubes or graphene exhibited high catalytic activities toward oxygen reduction reaction (ORR).[164–167]

3.3.1 Graphene as the support of Pt catalyst. Carbon materials are promising catalyst supports, due to their chemical inertness, wide electrochemical windows, and excellent charge mobilities.[162,168] Carbon black is the most widely used carbon based support because of its large SSA and low price. However, the aggregation of Pt nanoparticles and the corrosion of carbon black by oxygen during the cycling processes of fuel cells strongly reduce the electrocatalytic activities of the catalysts.[162] Carbon nanotubes have shown better stability than that of carbon black.[169] However, high-quality carbon nanotubes are also expensive. Thus, graphene has been exploited as the support of Pt catalyst. Liu *et al.* compared the SSA, electrocatalytic activity for ORR and stability of the Pt nanoparticles supported on the functionalized graphene sheets (Pt-FGS) and carbon blacks (*E*-TEK) under the same testing conditions.[40] Pt-FGS showed not only larger SSA and higher ORR activity, but also excellent stability after 5000 cyclic voltammetry cycles. These improved properties were attributed to the smaller aggregation of Pt particles immobilized on graphene. Besides, Pt nanoparticles were supported on graphene nanoplatelets, and this catalyst also showed a good electrochemical durability (2∼3 times that of the Pt/CNT or *E*-TEK Pt/C).[170]

The morphology and the dispersing state of Pt nanoparticles also influence their catalytic activities. LBL self-assembly is considered to be an effective approach for adjusting material structures on the nanometre scale.[171] An imidazolium salt-based ionic liquid functionalized graphene and platinum nanoparticles were LBL assembled into a 3D hybrid nanostructure. Pt nanoparticles were uniformly dispersed on the surfaces of graphene sheets and the composite exhibited high electrocatalytic activity for ORR. Furthermore, the electrocatalytic activity of the composite can be adjusted by its bilayer number. Yang *et al.* reported a green electrochemical approach for producing Pt/graphene composites.[172] Pt nanoparticles were uniformly deposited on graphene sheets as shown in Fig. 7a. The ORR current density at the composite electrode was measured to be much stronger than that at a Pt nanoparticle modified glassy carbon electrode. Furthermore, the onset potential of the ORR wave at the former electrode is also much higher than that at the latter electrode. Nitrogen doped carbon material is recognized as good support for Pt catalyst. The doped nitrogen atoms not only provide the anchoring sites for the metal particles, but also act as chemically active sites for catalytic reactions.[173] On the other

hand, the introduction of carbon materials can also increase the electron mobility of the catalyst support. Wu *et al.* prepared N-doped graphene by heating graphene oxide in an ammonia flow at various temperatures (300, 500, 700 and 800 °C).[173] The morphological comparison of the Pt nanoparticles supported on graphene and N-doped graphene is shown in Fig. 7c and 7d. The methanol oxidation current at the composite of Pt nanoparticles and the N-doped graphene treated by heating at 800 °C (135 mA mg^{-1}) was tested to be threefold higher than those at the other three composites (heated at 300, 500 or 700 °C). It was also much stronger than that at a commercial Pt/CB catalyst (27 mA mg^{-1}). This is mainly due to the composite treated at high temperature (*e.g.*, 800 °C) having higher conductivity than the other samples and Pt nanoparticles being more uniformly dispersed on its surface. Ramaprabhu and co-workers also investigated the nitrogen doped graphene nanoplatelets as the catalyst support of Pt for ORR.[174] In this case, the nitrogen doped graphene was made by nitrogen plasma treatment of graphene. The fuel cells with Pt/N-doped graphene and Pt/graphene composite catalysts achieved power densities of 440 and 390 mW cm^{-2}, respectively.

Beside spherical nanoparticles, Pt nanodentrites are expected to be a potential catalyst of fuel cells because of their high SSA and conductivity. A composite of Pt-on-Pd bimetallic nanodendrites and graphene sheets was synthesized and its catalytic activity on methanol oxidation was investigated (Fig. 7b).[42] The current density of methanol oxidation catalyzed by this composite is about 3.0 or 9.5 times higher than that by a Pt black or *E*-TEK Pt/C catalyst.

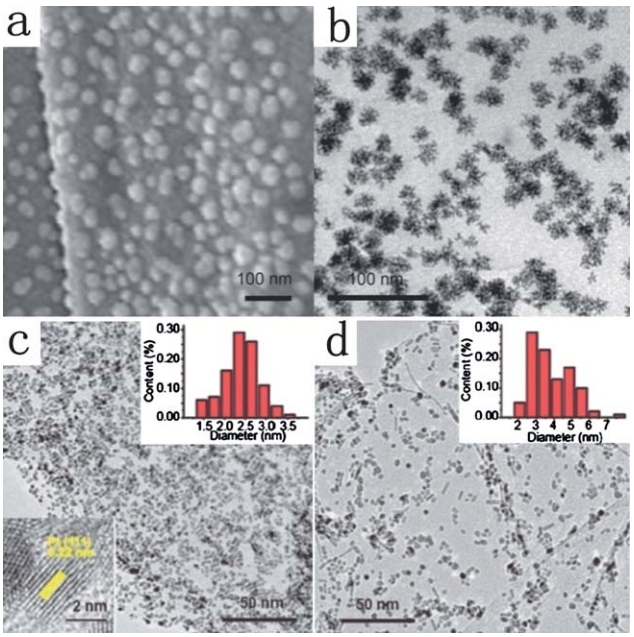

Fig. 7 (a) SEM image of the Pt particles supported on graphene sheets by electrodeposition, reproduced with permission from ref. 172 © 2010 Elsevier B.V. (b) TEM image of the Pt nanodentrites supported on graphene sheets, reproduced with permission from ref. 42 © 2010 American Chemical Society. (c, d) TEM images of Pt nanoparticles supported on (c) the N-doped and (d) pure graphene sheets, reproduced from ref. 173 with permission of the *PCCP* Owner Societies, © 2010 Royal Society of Chemistry.

Another problem of using Pt catalyst in fuel cells is that the catalyst can be poisoned by carbon monoxide (CO), a byproduct produced during oxidizing carbon hydroxides such as methanol and ethanol.[23] One of the solutions to this problem is the use of Pt based alloys as catalysts. Dong *et al.* studied the electrocatalytic activity of the graphene supported Pt–Ru nanoparticles for methanol and ethanol oxidations.[175] Compared to the widely used Vulcan XC-72R carbon black, graphene strongly enhanced the oxidation efficiencies of both methanol and ethanol. Furthermore, the introduction of Ru greatly reduced the adsorption of CO-like carbonaceous species on the surfaces of Pt particles.

3.3.2 Nitrogen doped graphene. Various metal free materials were also exploited for replacing Pt as the catalysts of fuel cells. Nitrogen doped carbon materials (*e.g.* carbon nanotubes, graphene) and graphitic carbon nitride were found to be good catalysts for ORR.[88,164–167] Nitrogen doped graphene can be synthesized by chemical vapor deposition of methane in the presence of ammonia as reported by Dai *et al.*[166] Compared to the commercialized platinum catalysts, this material showed higher electrocatalytic activity, longer term stability, and improved tolerance to CO for ORR. Considering the low price and high electrocatalytic activity, nitrogen doped graphene can be used as an efficient ORR catalyst for fuel cells. Another example of nitrogen doped graphene catalyst was reported by Lin and co-workers. They synthesized this material by exposing graphene to nitrogen plasma.[167] Graphene prepared by reducing graphene oxide with hydrazine also contained C=N bonds and showed electrocatalytic activity to ORR.[176]

3.4 Water splitting

Hydrogen is regarded as an ultimate clean fuel, and the production of hydrogen with solar power plays an important role in clean and renewable energy systems.[177,178] Among all solar-to-hydrogen conversion methods, direct splitting water by a photocatalyst is of the most convenience.[179] However, the practical applications of this technique are limited by the inability to utilize visible light, insufficient quantum efficiency and/or photodegradation of the catalyst.[180] Designing novel catalysts to meet the industrial needs is still a challenge.

Owing to its superior electron mobility and high SSA, graphene was considered to be a high performance support for photocatalysts. Kamat and co-workers demonstrated the feasibility of using graphene as an electron-transfer medium.[181] As shown in Fig. 8a, the transparent dispersion of TiO_2 nanoparticles in deaerated ethanol changed to blue upon illumination with UV light, mainly due to the adsorption of trapped photoelectrons on TiO_2 nanoparticles. Then, a deaerated dispersion of graphene oxide was added into this system. As a result, the blue color of the TiO_2 nanoparticles with trapped electrons gradually disappeared. During this process, graphene oxide was spontaneously reduced to r-GO, indicating a successful charge transfer from TiO_2 to graphene oxide. Successively, a controlled amount of $AgNO_3$ solution was added. Without further illumination, Ag^+ was readily reduced to Ag nanoparticles anchored on graphene sheets, resulting in the formation of a ternary nanocomposite. This phenomenon provides a strong evidence of

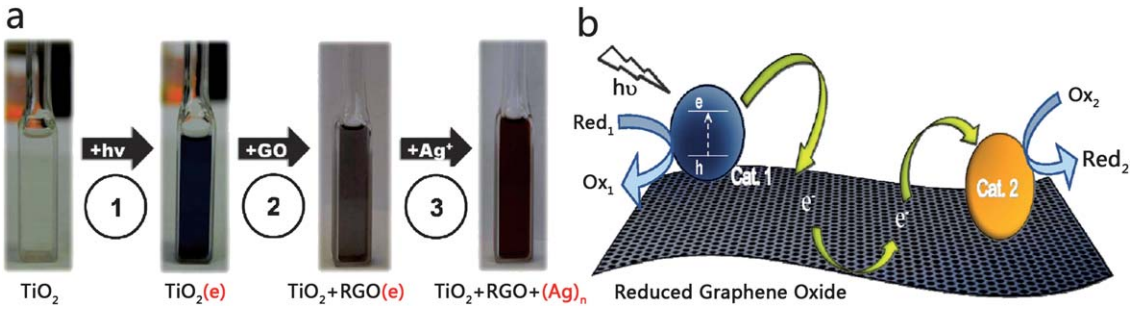

Fig. 8 (a) Digital photographs indicate the electron transfer from illuminated TiO_2 to graphene oxide, and then to Ag^+, and (b) schematic illustration of the electron transportation on graphene, reproduced with permission from ref. 181 © 2010 American Chemical Society.

graphene being able to store and transport photoelectrons for further reduction reaction (Fig. 8b). Therefore, graphene is believed to be effective for preventing the electron-hole recombination by accepting and transporting photoelectrons, and inhibiting the backward reaction by separating the evolution sites of hydrogen and oxygen.[182]

Cui *et al.* evaluated the photocatalytic performance of a graphene/TiO_2 nanocomposite containing 5 wt% graphene.[45] In this study, the hydrogen evolution was tested by illuminating the composite powder suspension with a Xe lamp in the presence of sacrificial agents (Na_2S and Na_2SO_3). The hydrogen evolution rate of this system was measured to be 8.6 μmol h^{-1} and this value was nearly twice that of the system with pure commercial TiO_2 catalyst (P25). In another system, graphene was introduced to a visible-light driven $BiVO_4$ photocatalyst for photo-electrochemical water-splitting.[43] Compared with pure $BiVO_4$, the photoanode based on graphene/$BiVO_4$ composite showed nearly 10-fold enhancement of photocurrent at a 0.8 V bias. Graphene sheets facilitated the electron transport between illuminated $BiVO_4$ and the electrode; thus, they partly prevented the recombination of photo-electrons and holes. The incident photon-to-current-conversion efficiency (IPCE) of the composite was measured to be 4.2%, which is significantly larger than that of pure $BiVO_4$ (0.3%).

Furthermore, graphene itself might become a next generation photocatalyst. Perfect graphene sheet is a gapless semiconductor with no photocatalytic activity. However, the band gap of graphene sheets can be modulated by functionalization or cutting them into nanoribbons.[8,183] Graphene oxide, as an oxygen-functionalized semiconducting graphene with a band gap of 2.4∼4.3 eV, has been applied as a photocatalyst for generating hydrogen upon illumination with visible light (Fig. 9).[44]

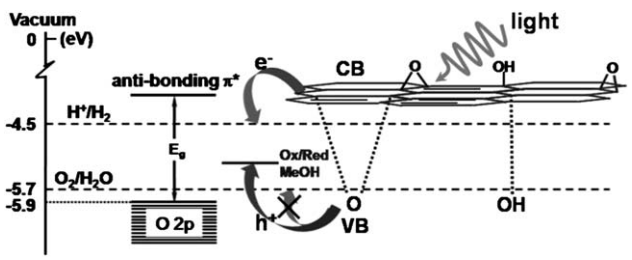

Fig. 9 Energy-levels of semiconducting graphene oxide showing it is a promising catalyst for water splitting, reproduced with permission from ref. 44 © 2010 Wiley-VCH.

Although a sacrificial agent is demanded, graphene oxide showed a stable photocatalytic hydrogen evolution activity of 210 or 41 mmol h^{-1} under mercury or visible-light irradiation, respectively. Moreover, in this case, the hydrogen evolution rate did not decrease obviously after illumination for 50 h, even though graphene oxide was photo-reduced to graphene in the same process.

3.5 Solar cells

Solar cell can directly convert solar energy to electrical power. Thus, it is one of the most promising devices satisfying the global energy requirements. As a novel and unique member of carbon nanomaterials, graphene manifests attractive application potentials in transparent electrodes, dye-sensitized as well as heterojunction solar cells.[8,9,33,34,184]

3.5.1 Transparent electrodes. Transparent electrode (TE) is a fundamental component for both thin-film and dye-sensitized solar cells. A good TE should possess low sheet resistance, high transparency and proper work function. Currently, the most widely used TEs including indium tin oxide (ITO) and fluorine tin oxide (FTO) perform well in these aspects. However, they suffer from many deficiencies such as high production costs, limited resource of indium, ion diffusion into polymer layers and brittle structures.[184] Several other mostly developed high-performance TEs (*e.g.* single-walled CNT or metal nanowires) are also expensive.[185] Therefore, alternative materials for TEs are urgently required for the development of high performance solar cells. The rise of graphene, a single-layer graphite with high theoretical conductivity and good transparency (transmittance = 97.7%), is an attractive candidate to meet this purpose, especially for ultra-thin and flexible photovoltaic devices.[5,184,186,187] Moreover, graphene-based TEs can be fabricated *via* inexpensive solution-based methods,[19] and their work function could also be engineered *via* chemical doping or structural engineering.[188] However, achieving a graphene based TE with both high transparency and conductivity is a challenging task, for improving the conductivity usually results in reducing the transparency and *vice versa*.

Generally, there are two strategies to prepare graphene based TEs: solution-based assembly of chemically converted graphene (CCG) sheets into thin films and synthesizing large-size continuous graphene sheets. In comparison, the former route has several advantages described as follows. On the one hand, the

starting material of CCG is usually low-cost and abundant graphite; on the other hand, it is facile to process CCG sheets into a large area film *via* wet processing techniques (*e.g.* spin-coating, dip-coating, filtration or self-assembly). Furthermore, CCG can be easily blended with other functional materials into composite films. Graphene based TEs prepared by a variety of wet processing techniques as well as post treatments (doping or defect repair) have been reported.[36,81–83,189–195] However, their conductivities and transparencies are still far from the requirements of practical applications (sheet resistance <100 Ω/□ at T > 90%, Fig. 10).

The low conductivities of assembled CCG thin films are mainly attributed to two factors: structural defects of each CCG sheet and contact resistance between different sheets. Therefore, maximally reconstructing the conjugated structures of CCG sheets is of great importance. Up-to-date, the most effective approaches to remove the oxygenated groups of graphene oxide sheets and restore their conjugated structures include reducing them with hydroiodic acid and annealing them at high temperatures and under ultra-high vacuum conditions.[195–197] Carbon vacancy defects of CCG sheets could also be partly restored by annealing them in a healing agent (*e.g.* acetylene) atmosphere.[192,193,198] Exfoliating graphite in solutions without severe oxidation is also a practical method to avoid the generation of defects in graphene sheets. A high performance TE (10^2 Ω/□ at T = 70%) has been reported by self-assembling non-oxidized graphene sheets at a liquid/liquid interface.[199] However, the elaborate process and unsatisfactory yield of this method limit its application, as discussed in section 2.1.

Since the solution processed TEs are usually formed through assembling small CCG sheets, the inter-sheet resistance is a crucial factor for limiting their conductivities. Two strategies have been applied for reducing the inter-sheet resistance of CCG films. The first one is enlarging the sizes of CCG sheets to reduce the total number of inter-layer contacts. A TE based on large-size r-GO showed a resistance of 840 Ω/□ at T = 78%, which is much smaller than that based on small sheets (19.1 kΩ/□ at T = 79%).[195] Another route is bridging the CCG sheets by other conducting nanomaterials. For example, the TE fabricated by spin-coating a CCG/CNT hybrid dispersion showed a greatly enhanced performance (636 Ω/□ at T = 92%), which is superior to that of the TE based on either CNT or graphene.[201] Doping the graphene sheet with $SOCl_2$ or I_2 further reduced the resistance of this composite TE to 260 Ω/□ at T = 88%. These values are close to those of the commercial requirements while the production cost of this graphene/CNT composite electrode is low. The synergic effect of graphene and CNT has also been investigated by adding a small proportion of graphene sheets (~3 wt%) into CNT-based TE.[189] The graphene sheets were effectively circumvented the poor inter-tube contacts between CNTs; increasing the conductivity of the composite.

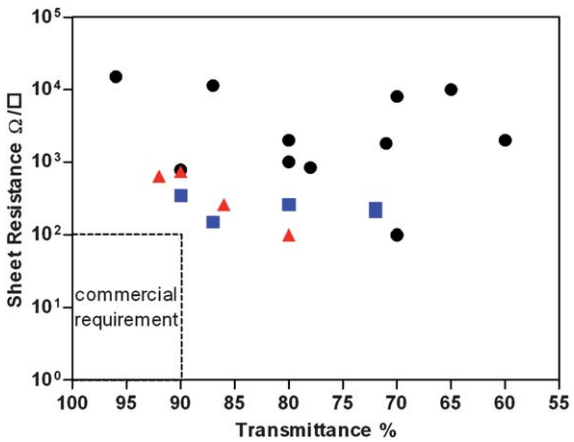

Fig. 10 Comparison of transmittances and sheet resistance of the graphene films prepared by different methods: solution-based processing (black dots), CVD (blue squares) and graphene/CNT composite (red triangles) according to literature sorces.[36,52,53,81–83,185,193,195,198–205]

Solution-assembled graphene TEs will finally meet a bottleneck for their inter-sheet resistance. However, the production of large-area continuous graphene sheets can circumvent this problem. Chemical vapor deposition (CVD) on metal foils is the most practical route to high-quality, transferable and/or patterned graphene films.[52,53,203] The performance of CVD graphene TEs greatly exceeds that of the solution-processed counterparts, as compared in Fig. 10. Graphene grown on copper foil possesses a single-layer structure in its most areas, and the TE prepared by transferring it onto a poly(methyl methacrylate) (PMMA) substrate exhibited a resistance of 350 Ω/□ at T = 90% as well as good conductivity retention after repeated bending.[53] Multi-layered graphene prepared by CVD on Ni is even more stretchable (up to 11% elongation) after transferring to a poly(dimethyl siloxane) (PDMS) substrate.[52] Doping CVD grown graphene with $AuCl_3$ further increases its performance to 150 Ω/□ at T = 87%, which is close to the required value for real application.[203] Except for CVD, cooling the carbon/metal solution can also produce a large-area multi-layered graphene film. The film has a resistance of 200 Ω/□ at T = 85%, which is comparable to that of CVD grown graphene.[206]

The performance of the solar cells with graphene-based TEs are summarized in Table 4.[36,54,82,189,190,205] It is clear from this table that the cell performances with different graphene based TEs are in following order: solution-processed graphene ≪ CVD grown graphene <ITO, which is in accordance with the quality sequence of TEs. However, the energy conversion efficiencies of the solar cells with ITO electrodes are irreversibly deteriorated after bending, while those of the cells with graphene electrodes changed little.

3.5.2 GBMs for dye-sensitized solar cells. Dye-sensitized solar cells (DSSCs) have attracted a great deal of attention because of their low cost, convenient manufacturing process and comparable efficiencies to those of amorphous silicon solar cells. A DSSC consists of a transparent electrode as photoanode, a mesoporous semiconductor (usually TiO_2) layer, a monolayer of dye, an electrolyte containing redox pairs (usually I_2/I_3^-), and a counter electrode. The details about the structure and function of each component are described in the literature.[20,207,208] The prospect of DSSC is attractive; however, its practical applications require improvements on several aspects: replacing expensive ruthenium-based dyes and platinum-based counter electrodes, optimizing the structures of TiO_2 layers, developing liquid-free electron donators and fabricating high-performance flexible photoanodes.[207–210] Recent research has shown that

Table 4 Performance of the solar cells with graphene-based TEs

Cell type	TE materials	η^a (%)	$J_{sc}{}^a$ (mA cm^{-2})	$V_{oc}{}^a$(V)	FF^a(%)	Ref.
Polymer photovoltaic	Solution-processed graphene	0.13	1.18	0.46	0.246	190
	ITO	3.59	12.32	0.6	0.486	
	Solution-processed graphene	1.01	4.18	0.67	0.36	82
	ITO	2.04	5.39	0.69	0.55	
	CVD graphene	0.21	2.39	0.32	0.27	54
	CVD graphene wetted	1.71	6.05	0.55	0.513	
	ITO	3.1	9.03	0.56	0.611	
Small molecular organic photovoltaic	Solution-processed graphene	0.4	2.1	0.48	0.37	189
	ITO	0.84	2.8	0.47	0.54	
	CVD graphene	1.18	4.73	0.48	0.52	205
	ITO	1.27	4.69	0.48	0.57	
Dye-sensitized solar cell	Solution-processed graphene	0.26	1.01	0.7	0.36	36
	FTO	0.84	3.02	0.76	0.36	

^{a} η, J_{sc}, V_{oc} and FF are power conversion efficiency, short-circuit current density, open circuit voltage and fill factor, respectively.

graphene is an attractive material for applying in most of these aspects.

3.5.2.1 Electron transport promoter for TiO_2 layer. The mesoporous TiO_2 layers are the heart components of most DSSCs, through which the photoelectrons generated from dye molecules are transported to the anodes.[20] Therefore, a recombination reaction (*i.e.* reverse charge transfer from TiO_2 to the dye or redox couple) severely reduces the cell efficiency. One effective way to promote charge transfer and reduce backward recombination is incorporating a conductive network into TiO_2. Thus, graphene shows incomparable potential not only for its extremely high carrier mobility but also for its unique 2D flexible structure.[87] Fig. 11 illustrates the structural advantage of 2D graphene. As shown in this figure, the interaction between 0D TiO_2 nanoparticles and 1D materials (*e.g.* CNT) is geometrically weaker than that between TiO_2 and 2D graphene.[87] The effective charge transfer from TiO_2 to graphene, as described in section 3.4, also indicates that graphene is a suitable electron transport promoter for DSSCs.[181,182] Recent research demonstrated that the incorporation of a small amount of graphene into TiO_2 layer significantly increased the power conversion efficiency of DSSC. The performance of TiO_2/graphene composite is much better than that of pure TiO_2 as well as TiO_2/CNT (at the same loading ratio), indicating that graphene is a good promoter for electron transportation.[87,211–213]

3.5.2.2 Counter electrodes. The duty of the counter electrode in a DSSC is catalyzing the reduction of I_2 after electron injection. In a DSSC, the reductions of I_2 at both the counter electrode and TiO_2 surface are competing; therefore, the electrocatalytic efficiency of the counter electrode should be as high as possible to inhibit the backward reaction. For practical applications, Pt-based electrode has to be replaced by inexpensive materials and highly conductive carbon based materials are promising candidates. For example, we synthesized a water-soluble noncovalent graphene functionalized by pyrenebutyrate (PB^-) and used it as the counter electrode material of DSSC.[39] The performance of PB^--graphene/FTO electrode greatly surpassed that of bare FTO, while it is inferior to that of a Pt/FTO electrode. Further improvement was achieved by blending polystyrenesulfonate doped poly(3,4-ethylenedioxythiophene) (PEDOT:PSS) with PB^--graphene.[38] The cell with a PEDOT:PSS/PB^--graphene counter electrode exhibited a comparable efficiency to that of the cell with a Pt cathode. Furthermore, the composite film is transparent and flexible, manifests an application potential in both flexible solar cells and power-producing windows.[38]

3.5.2.3 Graphene based dyes. The dye molecules used in DSSCs should possess proper band gaps, good charge injection to TiO_2, long-term stability and effective blocking of the I_2 reduction at TiO_2 surface. Recently, a great deal of effort has

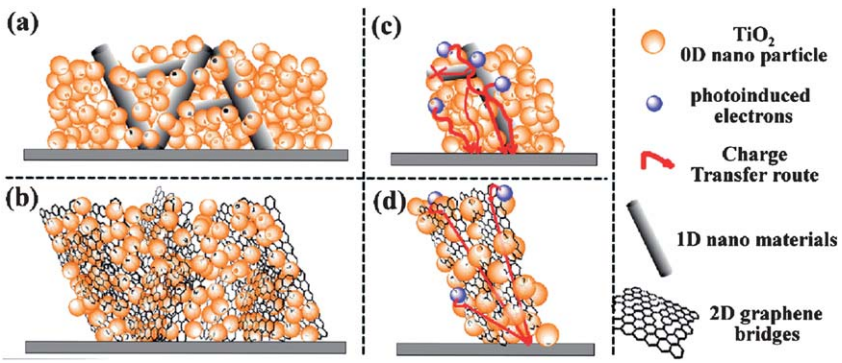

Fig. 11 Schematic illustration shows the charge transfer from 0D TiO_2 to 2D graphene (b, d) is more efficient than that to 1D materials (a, c), reproduced with permission from ref. 87 © 2010 American Chemical Society.

been devoted to searching for high-performance alternatives to ruthenium-based dyes.[207,210] As discussed in section 3.4, defect-free graphene is a zero bandgap semiconductor; however, reducing the size of a graphene sheet renders controllable band gaps between zero and that of benzene. Therefore, engineering the energy level of graphene might provide us with a new generation of dyes for DSSCs. Recently, an organically synthesized graphene quantum dot consisting of 67 aromatic rings was used as a dye molecule for DSSC.[66] The black-colored graphene quantum dots showed an absorption edge up to 900 nm. Even though the pioneering cell has a low efficiency because of the poor interaction between a dye molecule and TiO_2, its performance can be further improved by functional modification of graphene. In view of application, the organic synthesis of graphene is too expensive for practical application. Therefore, a top-down approach, from natural graphite to graphene quantum dots *via* exfoliation or structural cutting might be a promising route to graphene based dyes. Nevertheless, several factors listed as follows should be considered: controlling the energy levels of graphene quantum dots, preventing their unwanted restacking, improving their solution processibility, stability and affiliation with TiO_2.

3.5.3 GBMs for heterojunction solar cells. Heterojunction solar cells are devices that convert solar energy to electrical power *via* photovoltaic effect of p-n junctions, which can be simply divided into two types: inorganic and organic.[24] Inorganic (especially silicon based) cells usually possess high conversion efficiencies, but their production is usually elaborate, expensive, needs rigorous processing conditions, and not environmentally benign. In comparison, organic photovoltaics (OPV) manifest more advantages including solution processability, cost-effectiveness and light weight.[214] However, the conversion efficiency of the state-of-the-art OPVs is still much lower than that of silicon-based cells.[215]

On the basis of its superior electrical property, graphene has been investigated for applications in heterojunction solar cells during the past several years. Most research is focusing on replacing or cooperating with C_{60} derivatives as electron acceptors of polymer-based OPVs. The motivation mostly lies in the following aspects: first, an electron acceptor is a necessary component of polymer OPV. In the absence of an electron acceptor, the photo-generated exitons in conjugated polymers cannot be separated into electrons and holes.[24] Second, graphene-based materials have controllable band gaps and work functions, which could perfectly match the energy levels of conjugated polymers.[8] Third, the formation of continuous structures of both donor and acceptor will improve the charge transport efficiencies toward electrodes, and, 0D fullerene derivatives are theoretically inferior to 1D CNT or 2D graphene.[89] Furthermore, as the "mother" of all graphitic nanomaterials, graphene has the largest conjugated basal plane for binding conjugated polymers.[2] On the basis of these considerations, several functionalized graphene materials have been applied as the electron acceptors for poly(3-hexylthiophene) (P3HT) and poly(3-octylthiophene) (P3OT) based solar cells. For example, graphene was functionalized by phenyl isocyanate or butylamine to provide its solubility, and then blended with P3HT or P3OT.[89,216] The as-prepared P3OT/graphene solar cell (Fig. 12a) showed a 0.32% power conversion efficiency; after annealing, however, the efficiency further increased to 1.4%, mainly due to the removal of functional groups from the graphene component and the improvements in the morphology and crystallinity of the P3OT component.[89] The graphene/P3HT solar cell also showed a similar efficiency of 1.1%.[37,217] This value is quite lower than the state-of-the-art OPVs, which might be due to the irregular molecular structure of the r-GO; however, graphene based cells exhibited higher efficiencies than those of the CNT based counterparts. Furthermore, a theoretical study predicts that the graphene-based OPV may have an efficiency of over 12% for a single cell; therefore, it is strongly expected for graphene to break through the bottleneck of OPVs with further optimization.[218]

GBMs have also been applied as the other components of heterojunction solar cells. First, the electron delocalization of P3HT can be enhanced *via* grafting the polymer chains to graphene sheet. In this case, graphene acted as a promoter for electron transportation. For example, a bilayer solar cell based on P3HTgrafted graphene showed 200% higher power conversion efficiency than that of pure P3HT/C_{60} cell.[219] Second, graphene oxide was used to replace the mostly used hole transport material, PEDOT:PSS. An ultrathin graphene oxide transport layer (2 nm) exhibited a comparable performance to that of PEDOT:PSS. However, graphene oxide film has the advantages of a facile production process and low cost.[220] Third, a novel layered graphene/CdS quantum dot composite photovoltaic electrochemical cell was fabricated. This cell has shown an external quantum yield of 16%, which is higher than that of the cell fabricated from a single-walled CNT/CdS composite. The improved performance of the graphene-based cell is ascribed to the strong interaction between graphene and 0D CdS nanoparticles and the matched energy levels of both components.[84,221] Besides, graphene has also been investigated as an electron donor in photovoltaics. A device with a synthetic nanographene as

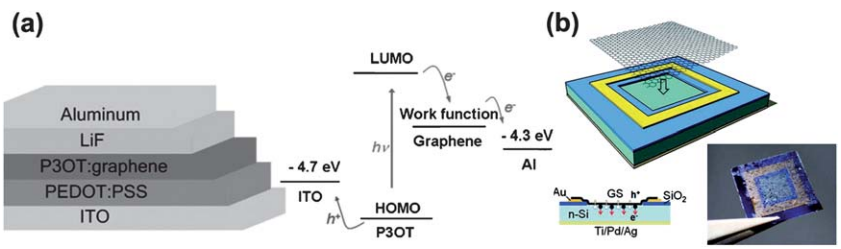

Fig. 12 (a) Structure of a P3OT/graphene photovoltaic cell with the corresponding energy level diagram, reproduced with permission from ref. 89 © 2008 Wiley-VCH. (b) Fabrication and photograph of a graphene/n-silicon cell, reproduced with permission from ref. 222 © 2010 Wiley-VCH.

donor and a perylenetetracarboxydiimide derivative as acceptor exhibited an external quantum efficiency up to 19%.[65] Moreover, with a similar structure to that of heterojunction cells, a Schottky-junction solar cell based on graphene/n-silicon was facilely constructed, as illustrated in Fig. 12b.[222] By transferring a graphene film directly onto a pretreated n-type silicon/SiO_2 wafer, a solar cell with an energy conversion efficiency of 1.65% was achieved. In this cell, graphene has multifunctions: a component of Schottky junction, hole transporting layer and transparent electrode. If the graphene layer was replaced by a graphene/CNT composite film with a bilayer structure, the efficiency of the CNT/graphene/n-Si ternary heterojunction solar cell further increased to 5.2%.[204] In the latter device, CNTs improved the charge separation and hole transportation of graphene, and graphene served as an intermediate layer for connecting CNTs with n-Si layer. In view of the versatile applications described above, graphene is expected to be a promising material for fabricating high-performance solar cells.

4. Conclusions

Carbon nanomaterials including carbon nanotubes, fullerene and its derivatives, carbon black and graphene have been widely applied in energy related systems. Among them, graphene is attractive because of its unique atom-thick 2D structure and excellent electrical, thermal, mechanical and optical properties. Furthermore, it has high chemical and electrochemical stabilities, and can be produced on a large scale at low cost. Thus, graphene is regarded as a promising material for the storage and conversion of renewable energies. Herein, we have systematically reviewed the synthesis of GBMs and their applications in supercapacitors, solar cells, fuel cells and water splitting.

Although considerable progress has been achieved, the studies in this field are in their primary stages; at least, the following challenges still remained. First, the performance of GBMs is limited by their SSAs and conductivity. Although the SSA and conductivity of single-layer perfect graphene are extraordinarily high, most practical GBMs have structural defects and their surfaces cannot be fully exposed due to the strong restacking tendency of graphene sheets. Second, the chemical and physical stabilities of GBMs still need improvement. For example, the lithium storage capacities of GBMs are greatly decreased in cycling tests. In composite electrodes for supercapacitors, LIBs as well as fuel cells, the structures of graphene-based scaffolds should be constructed perfectly to prevent the nanoparticles or conducting polymers from swelling, shrinkage and agglomeration. Third, the mechanisms of the GBMs working in energy related systems are partly unclear. For example, the explanations of lithium storage in graphene or its composites are controversial. The applications of graphene in solar cells and photocatalysts are also at their initial stages: the effects of graphene are mainly postulated and the performance of GBMs is usually far below the state-of-the-art counterparts. Nevertheless, nowadays researchers in the world believe that many bottlenecks of current clean and renewable energy devices can be broken through using GBMs. After fully exploring the potential of graphene, a revolution of clean and renewable energy materials will be realized.

Acknowledgements

This work was supported by the Natural Science Foundation of China (50873052 and 20774056).

References

1 K. S. Novoselov, A. K. Geim, S. V. Morozov, D. Jiang, Y. Zhang, S. V. Dubonos, I. V. Grigorieva and A. A. Firsov, *Science*, 2004, **306**, 666–669.
2 A. K. Geim and K. S. Novoselov, *Nat. Mater.*, 2007, **6**, 183–191.
3 J. H. Chen, C. Jang, S. D. Xiao, M. Ishigami and M. S. Fuhrer, *Nat. Nanotechnol.*, 2008, **3**, 206–209.
4 A. A. Balandin, S. Ghosh, W. Z. Bao, I. Calizo, D. Teweldebrhan, F. Miao and C. N. Lau, *Nano Lett.*, 2008, **8**, 902–907.
5 R. R. Nair, P. Blake, A. N. Grigorenko, K. S. Novoselov, T. J. Booth, T. Stauber, N. M. R. Peres and A. K. Geim, *Science*, 2008, **320**, 1308–1308.
6 C. Lee, X. D. Wei, J. W. Kysar and J. Hone, *Science*, 2008, **321**, 385–388.
7 M. D. Stoller, S. J. Park, Y. W. Zhu, J. H. An and R. S. Ruoff, *Nano Lett.*, 2008, **8**, 3498–3502.
8 F. Bonaccorso, Z. Sun, T. Hasan and A. C. Ferrari, *Nat. Photonics*, 2010, **4**, 611–622.
9 G. Eda and M. Chhowalla, *Adv. Mater.*, 2010, **22**, 2392–2415.
10 Q. Wu, Y. X. Xu, Z. Y. Yao, A. R. Liu and G. Q. Shi, *ACS Nano*, 2010, **4**, 1963–1970.
11 E. Yoo, J. Kim, E. Hosono, H. Zhou, T. Kudo and I. Honma, *Nano Lett.*, 2008, **8**, 2277–2282.
12 D. Chen, L. H. Tang and J. H. Li, *Chem. Soc. Rev.*, 2010, **39**, 3157–3180.
13 H. Bai, Y. X. Xu, L. Zhao, C. Li and G. Q. Shi, *Chem. Commun.*, 2009, 1667–1669.
14 S. Stankovich, D. A. Dikin, G. H. B. Dommett, K. M. Kohlhaas, E. J. Zimney, E. A. Stach, R. D. Piner, S. T. Nguyen and R. S. Ruoff, *Nature*, 2006, **442**, 282–286.
15 D. A. Dikin, S. Stankovich, E. J. Zimney, R. D. Piner, G. H. B. Dommett, G. Evmenenko, S. T. Nguyen and R. S. Ruoff, *Nature*, 2007, **448**, 457–460.
16 H. Chen, M. B. Muller, K. J. Gilmore, G. G. Wallace and D. Li, *Adv. Mater.*, 2008, **20**, 3557–3561.
17 Y. Xu, W. Hong, H. Bai, C. Li and G. Shi, *Carbon*, 2009, **47**, 3538–3543.
18 X. L. Wang, H. Bai, Z. Y. Yao, A. R. Liu and G. Q. Shi, *J. Mater. Chem.*, 2010, **20**, 9032–9036.
19 S. Park and R. S. Ruoff, *Nat. Nanotechnol.*, 2009, **4**, 217–224.
20 M. Gratzel, *J. Photochem. Photobiol., C*, 2003, **4**, 145–153.
21 B. Coelho, A. C. Oliveira and A. Mendes, *Energy Environ. Sci.*, 2010, **3**, 1398–1405.
22 M. Winter and R. J. Brodd, *Chem. Rev.*, 2004, **104**, 4245–4269.
23 A. S. Arico, P. Bruce, B. Scrosati, J. M. Tarascon and W. Van Schalkwijk, *Nat. Mater.*, 2005, **4**, 366–377.
24 H. Spanggaard and F. C. Krebs, *Sol. Energy Mater. Sol. Cells*, 2004, **83**, 125–146.
25 P. J. Hall, M. Mirzaeian, S. I. Fletcher, F. B. Sillars, A. J. R. Rennie, G. O. Shitta-Bey, G. Wilson, A. Cruden and R. Carter, *Energy Environ. Sci.*, 2010, **3**, 1238–1251.
26 C. Liu, F. Li, L. P. Ma and H. M. Cheng, *Adv. Mater.*, 2010, **22**, E28–E62.
27 G. M. Scheuermann, L. Rumi, P. Steurer, W. Bannwarth and R. Mulhaupt, *J. Am. Chem. Soc.*, 2009, **131**, 8262–8270.
28 Y. J. Huang, Y. W. Qin, Y. Zhou, H. Niu, Z. Z. Yu and J. Y. Dong, *Chem. Mater.*, 2010, **22**, 4096–4102.
29 J. T. Robinson, F. K. Perkins, E. S. Snow, Z. Q. Wei and P. E. Sheehan, *Nano Lett.*, 2008, **8**, 3137–3140.
30 W. J. Hong, H. Bai, Y. X. Xu, Z. Y. Yao, Z. Z. Gu and G. Q. Shi, *J. Phys. Chem. C*, 2010, **114**, 1822–1826.
31 S. Park, N. Mohanty, J. W. Suk, A. Nagaraja, J. H. An, R. D. Piner, W. W. Cai, D. R. Dreyer, V. Berry and R. S. Ruoff, *Adv. Mater.*, 2010, **22**, 1736–1740.
32 H. Bai, C. Li, X. L. Wang and G. Q. Shi, *Chem. Commun.*, 2010, **46**, 2376–2378.
33 Y. H. Hu, H. Wang and B. Hu, *ChemSusChem*, 2010, **3**, 782–796.

34 M. H. Liang, B. Luo and L. J. Zhi, *Int. J. Energy Res.*, 2009, **33**, 1161–1170.
35 Y. X. Xu, Q. Wu, Y. Q. Sun, H. Bai and G. Q. Shi, *ACS Nano*, 2010, **4**, 7358–7362.
36 X. Wang, L. J. Zhi and K. Mullen, *Nano Lett.*, 2008, **8**, 323–327.
37 Q. Liu, Z. F. Liu, X. Y. Zhang, N. Zhang, L. Y. Yang, S. G. Yin and Y. S. Chen, *Appl. Phys. Lett.*, 2008, **92**, 223303.
38 W. J. Hong, Y. X. Xu, G. W. Lu, C. Li and G. Q. Shi, *Electrochem. Commun.*, 2008, **10**, 1555–1558.
39 Y. X. Xu, H. Bai, G. W. Lu, C. Li and G. Q. Shi, *J. Am. Chem. Soc.*, 2008, **130**, 5856–5857.
40 R. Kou, Y. Y. Shao, D. H. Wang, M. H. Engelhard, J. H. Kwak, J. Wang, V. V. Viswanathan, C. M. Wang, Y. H. Lin, Y. Wang, I. A. Aksay and J. Liu, *Electrochem. Commun.*, 2009, **11**, 954–957.
41 B. Seger and P. V. Kamat, *J. Phys. Chem. C*, 2009, **113**, 7990–7995.
42 S. J. Guo, S. J. Dong and E. W. Wang, *ACS Nano*, 2010, **4**, 547–555.
43 Y. H. Ng, A. Iwase, A. Kudo and R. Amal, *J. Phys. Chem. Lett.*, 2010, **1**, 2607–2612.
44 T. F. Yeh, J. M. Syu, C. Cheng, T. H. Chang and H. S. Teng, *Adv. Funct. Mater.*, 2010, **20**, 2255–2262.
45 X. Y. Zhang, H. P. Li, X. L. Cui and Y. H. Lin, *J. Mater. Chem.*, 2010, **20**, 2801–2806.
46 S. M. Paek, E. Yoo and I. Honma, *Nano Lett.*, 2009, **9**, 72–75.
47 D. H. Wang, D. W. Choi, J. Li, Z. G. Yang, Z. M. Nie, R. Kou, D. H. Hu, C. M. Wang, L. V. Saraf, J. G. Zhang, I. A. Aksay and J. Liu, *ACS Nano*, 2009, **3**, 907–914.
48 M. J. Allen, V. C. Tung and R. B. Kaner, *Chem. Rev.*, 2010, **110**, 132–145.
49 C. Berger, Z. M. Song, T. B. Li, X. B. Li, A. Y. Ogbazghi, R. Feng, Z. T. Dai, A. N. Marchenkov, E. H. Conrad, P. N. First and W. A. de Heer, *J. Phys. Chem. B*, 2004, **108**, 19912–19916.
50 C. Berger, Z. M. Song, X. B. Li, X. S. Wu, N. Brown, C. Naud, D. Mayou, T. B. Li, J. Hass, A. N. Marchenkov, E. H. Conrad, P. N. First and W. A. de Heer, *Science*, 2006, **312**, 1191–1196.
51 X. S. Li, W. W. Cai, J. H. An, S. Kim, J. Nah, D. X. Yang, R. Piner, A. Velamakanni, I. Jung, E. Tutuc, S. K. Banerjee, L. Colombo and R. S. Ruoff, *Science*, 2009, **324**, 1312–1314.
52 K. S. Kim, Y. Zhao, H. Jang, S. Y. Lee, J. M. Kim, J. H. Ahn, P. Kim, J. Y. Choi and B. H. Hong, *Nature*, 2009, **457**, 706–710.
53 X. S. Li, Y. W. Zhu, W. W. Cai, M. Borysiak, B. Y. Han, D. Chen, R. D. Piner, L. Colombo and R. S. Ruoff, *Nano Lett.*, 2009, **9**, 4359–4363.
54 Y. Wang, X. H. Chen, Y. L. Zhong, F. R. Zhu and K. P. Loh, *Appl. Phys. Lett.*, 2009, **95**, 063302.
55 D. H. Deng, X. L. Pan, H. Zhang, Q. A. Fu, D. L. Tan and X. H. Bao, *Adv. Mater.*, 2010, **22**, 2168–2171.
56 D. Li, M. B. Muller, S. Gilje, R. B. Kaner and G. G. Wallace, *Nat. Nanotechnol.*, 2008, **3**, 101–105.
57 S. Park, J. H. An, I. W. Jung, R. D. Piner, S. J. An, X. S. Li, A. Velamakanni and R. S. Ruoff, *Nano Lett.*, 2009, **9**, 1593–1597.
58 D. R. Dreyer, S. Park, C. W. Bielawski and R. S. Ruoff, *Chem. Soc. Rev.*, 2010, **39**, 228–240.
59 Y. Zhu, S. Murali, W. Cai, X. Li, J. W. Suk, J. R. Potts and R. S. Ruoff, *Adv. Mater.*, 2010, **22**, 3906–3924.
60 Y. Hernandez, V. Nicolosi, M. Lotya, F. M. Blighe, Z. Y. Sun, S. De, I. T. McGovern, B. Holland, M. Byrne, Y. K. Gun'ko, J. J. Boland, P. Niraj, G. Duesberg, S. Krishnamurthy, R. Goodhue, J. Hutchison, V. Scardaci, A. C. Ferrari and J. N. Coleman, *Nat. Nanotechnol.*, 2008, **3**, 563–568.
61 A. B. Bourlinos, V. Georgakilas, R. Zboril, T. A. Steriotis and A. K. Stubos, *Small*, 2009, **5**, 1841–1845.
62 X. L. Li, G. Y. Zhang, X. D. Bai, X. M. Sun, X. R. Wang, E. Wang and H. J. Dai, *Nat. Nanotechnol.*, 2008, **3**, 538–542.
63 C. Valles, C. Drummond, H. Saadaoui, C. A. Furtado, M. He, O. Roubeau, L. Ortolani, M. Monthioux and A. Penicaud, *J. Am. Chem. Soc.*, 2008, **130**, 15802–15804.
64 Y. B. Tang, C. S. Lee, Z. H. Chen, G. D. Yuan, Z. H. Kang, L. B. Luo, H. S. Song, Y. Liu, Z. B. He, W. J. Zhang, I. Elello and S. T. Lee, *Nano Lett.*, 2009, **9**, 1374–1377.
65 X. L. Feng, M. Y. Liu, W. Pisula, M. Takase, J. L. Li and K. Mullen, *Adv. Mater.*, 2008, **20**, 2684–2689.
66 X. Yan, X. Cui, B. S. Li and L. S. Li, *Nano Lett.*, 2010, **10**, 1869–1873.
67 X. Wang, L. J. Zhi, N. Tsao, Z. Tomovic, J. L. Li and K. Mullen, *Angew. Chem., Int. Ed.*, 2008, **47**, 2990–2992.
68 L. L. Zhang, R. Zhou and X. S. Zhao, *J. Mater. Chem.*, 2010, **20**, 5983–5992.
69 Y. C. Si and E. T. Samulski, *Chem. Mater.*, 2008, **20**, 6792–6797.
70 H. C. Schniepp, J. L. Li, M. J. McAllister, H. Sai, M. Herrera-Alonso, D. H. Adamson, R. K. Prud'homme, R. Car, D. A. Saville and I. A. Aksay, *J. Phys. Chem. B*, 2006, **110**, 8535–8539.
71 S. R. C. Vivekchand, C. S. Rout, K. S. Subrahmanyam, A. Govindaraj and C. N. R. Rao, *J. Chem. Sci.*, 2008, **120**, 9–13.
72 W. Lv, D. M. Tang, Y. B. He, C. H. You, Z. Q. Shi, X. C. Chen, C. M. Chen, P. X. Hou, C. Liu and Q. H. Yang, *ACS Nano*, 2009, **3**, 3730–3736.
73 Y. W. Zhu, S. Murali, M. D. Stoller, A. Velamakanni, R. D. Piner and R. S. Ruoff, *Carbon*, 2010, **48**, 2118–2122.
74 Y. X. Xu, K. X. Sheng, C. Li and G. Q. Shi, *ACS Nano*, 2010, **4**, 4324–4330.
75 P. Guo, H. H. Song and X. H. Chen, *J. Mater. Chem.*, 2010, **20**, 4867–4874.
76 J. Kim, L. J. Cote, F. Kim, W. Yuan, K. R. Shull and J. X. Huang, *J. Am. Chem. Soc.*, 2010, **132**, 8180–8186.
77 J. L. Vickery, A. J. Patil and S. Mann, *Adv. Mater.*, 2009, **21**, 2180–2184.
78 S. Bae, H. Kim, Y. Lee, X. F. Xu, J. S. Park, Y. Zheng, J. Balakrishnan, T. Lei, H. R. Kim, Y. I. Song, Y. J. Kim, K. S. Kim, B. Ozyilmaz, J. H. Ahn, B. H. Hong and S. Iijima, *Nat. Nanotechnol.*, 2010, **5**, 574–578.
79 Y. Y. Liang, D. Q. Wu, X. L. Feng and K. Mullen, *Adv. Mater.*, 2009, **21**, 1679–1683.
80 Y. Si and E. T. Samulski, *Nano Lett.*, 2008, **8**, 1679–1682.
81 H. A. Becerril, J. Mao, Z. Liu, R. M. Stoltenberg, Z. Bao and Y. Chen, *ACS Nano*, 2008, **2**, 463–470.
82 J. X. Geng, L. J. Liu, S. B. Yang, S. C. Youn, D. W. Kim, J. S. Lee, J. K. Choi and H. T. Jung, *J. Phys. Chem. C*, 2010, **114**, 8227–14440.
83 L. Zhao, Y. X. Xu, T. F. Qiu, L. J. Zhi and G. Q. Shi, *Electrochim. Acta*, 2009, **55**, 491–497.
84 C. X. Guo, H. B. Yang, Z. M. Sheng, Z. S. Lu, Q. L. Song and C. M. Li, *Angew. Chem., Int. Ed.*, 2010, **49**, 3014–3017.
85 L. J. Cote, F. Kim and J. X. Huang, *J. Am. Chem. Soc.*, 2009, **131**, 1043–1049.
86 S. Yang, X. Feng, S. Ivanovici and K. Müllen, *Angew. Chem., Int. Ed.*, 2010, **49**, 8408–8411.
87 N. L. Yang, J. Zhai, D. Wang, Y. S. Chen and L. Jiang, *ACS Nano*, 2010, **4**, 887–894.
88 Y. Q. Sun, C. Li, Y. X. Xu, H. Bai, Z. Y. Yao and G. Q. Shi, *Chem. Commun.*, 2010, **46**, 4740–4742.
89 Z. F. Liu, Q. Liu, Y. Huang, Y. F. Ma, S. G. Yin, X. Y. Zhang, W. Sun and Y. S. Chen, *Adv. Mater.*, 2008, **20**, 3924–3930.
90 H. Bai, L. Chun and G. Q. Shi, *Adv. Mater.*, 2011, **23**, DOI: 10.1002/adma.201003753.
91 J. Yan, T. Wei, B. Shao, Z. J. Fan, W. Z. Qian, M. L. Zhang and F. Wei, *Carbon*, 2010, **48**, 487–493.
92 S. Chen, J. W. Zhu, X. D. Wu, Q. F. Han and X. Wang, *ACS Nano*, 2010, **4**, 2822–2830.
93 K. Zhang, L. L. Zhang, X. S. Zhao and J. S. Wu, *Chem. Mater.*, 2010, **22**, 1392–1401.
94 A. R. Liu, C. Li, H. Bai and G. Q. Shi, *J. Phys. Chem. C*, 2010, **114**, 22783–22789.
95 J. Yan, Z. J. Fan, T. Wei, W. Z. Qian, M. L. Zhang and F. Wei, *Carbon*, 2010, **48**, 3825–3833.
96 D. W. Wang, F. Li, J. P. Zhao, W. C. Ren, Z. G. Chen, J. Tan, Z. S. Wu, I. Gentle, G. Q. Lu and H. M. Cheng, *ACS Nano*, 2009, **3**, 1745–1752.
97 Y. X. Xu, L. Zhao, H. Bai, W. J. Hong, C. Li and G. Q. Shi, *J. Am. Chem. Soc.*, 2009, **131**, 13490–13497.
98 D. S. Yu and L. M. Dai, *J. Phys. Chem. Lett.*, 2010, **1**, 467–470.
99 J. Yan, T. Wei, B. Shao, F. Q. Ma, Z. J. Fan, M. L. Zhang, C. Zheng, Y. C. Shang, W. Z. Qian and F. Wei, *Carbon*, 2010, **48**, 1731–1737.
100 R. Kotz and M. Carlen, *Electrochim. Acta*, 2000, **45**, 2483–2498.
101 B. E. Conway, V. Birss and J. Wojtowicz, *J. Power Sources*, 1997, **66**, 1–14.
102 J. S. Huang, B. G. Sumpter and V. Meunier, *Chem.–Eur. J.*, 2008, **14**, 6614–6626.
103 L. L. Zhang and X. S. Zhao, *Chem. Soc. Rev.*, 2009, **38**, 2520–2531.
104 A. G. Pandolfo and A. F. Hollenkamp, *J. Power Sources*, 2006, **157**, 11–27.

105 G. G. Wallace, J. Chen, D. Li, S. E. Moulton and J. M. Razal, *J. Mater. Chem.*, 2010, **20**, 3553–3562.
106 E. Frackowiak and F. Beguin, *Carbon*, 2001, **39**, 937–950.
107 S. Stankovich, D. Dikin, R. Piner, K. Kohlhaas, A. Kleinhammes, Y. Jia, Y. Wu, S. Nguyen and R. Ruoff, *Carbon*, 2007, **45**, 1558–1565.
108 Y. W. Zhu, M. D. Stoller, W. W. Cai, A. Velamakanni, R. D. Piner, D. Chen and R. S. Ruoff, *ACS Nano*, 2010, **4**, 1227–1233.
109 A. V. Murugan, T. Muraliganth and A. Manthiram, *Chem. Mater.*, 2009, **21**, 5004–5006.
110 X. A. Du, P. Guo, H. H. Song and X. H. Chen, *Electrochim. Acta*, 2010, **55**, 4812–4819.
111 Q. L. Du, M. B. Zheng, L. F. Zhang, Y. W. Wang, J. H. Chen, L. P. Xue, W. J. Dai, G. B. Ji and J. M. Cao, *Electrochim. Acta*, 2010, **55**, 3897–3903.
112 Y. Wang, Z. Q. Shi, Y. Huang, Y. F. Ma, C. Y. Wang, M. M. Chen and Y. S. Chen, *J. Phys. Chem. C*, 2009, **113**, 13103–13107.
113 Z. H. Tang, S. L. Shen, J. Zhuang and X. Wang, *Angew. Chem., Int. Ed.*, 2010, **49**, 4603–4607.
114 Y. Xu, Q. Wu, Y. Sun, H. Bai and G. Shi, *ACS Nano*, 2010, **4**, 7358, DOI: 10.1021/nn1027104.
115 A. P. Yu, I. Roes, A. Davies and Z. W. Chen, *Appl. Phys. Lett.*, 2010, **96**, 253105.
116 S. Biswas and L. T. Drzal, *ACS Appl. Mater. Interfaces*, 2010, **2**, 2293–2300.
117 Z. Fan, J. Yan, L. Zhi, Q. Zhang, T. Wei, J. Feng, M. Zhang, W. Qian and F. Wei, *Adv. Mater.*, 2010, **22**, 3723–2728.
118 H. L. Wang, H. S. Casalongue, Y. Y. Liang and H. J. Dai, *J. Am. Chem. Soc.*, 2010, **132**, 7472–7477.
119 P. Simon and Y. Gogotsi, *Nat. Mater.*, 2008, **7**, 845–854.
120 S. Chen, J. W. Zhu and X. Wang, *J. Phys. Chem. C*, 2010, **114**, 11829–11834.
121 J. X. Huang, S. Virji, B. H. Weiller and R. B. Kaner, *J. Am. Chem. Soc.*, 2003, **125**, 314–315.
122 C. Li, H. Bai and G. Q. Shi, *Chem. Soc. Rev.*, 2009, **38**, 2397–2409.
123 D. Li and R. B. Kaner, *Chem. Commun.*, 2005, 3286–3288.
124 M. H. Liang and L. J. Zhi, *J. Mater. Chem.*, 2009, **19**, 5871–5878.
125 S. Hossain, Y. K. Kim, Y. Saleh and R. Loutfy, *J. Power Sources*, 2006, **161**, 640–647.
126 H. Abe, T. Murai and K. Zaghib, *J. Power Sources*, 1999, **77**, 110–115.
127 S. H. Ng, J. Wang, Z. P. Guo, G. X. Wang and H. K. Liu, *Electrochim. Acta*, 2005, **51**, 23–28.
128 J. Chen, A. I. Minett, Y. Liu, C. Lynam, P. Sherrell, C. Wang and G. G. Wallace, *Adv. Mater.*, 2008, **20**, 566–570.
129 Y. S. Hu, P. Adelhelm, B. M. Smarsly, S. Hore, M. Antonietti and J. Maier, *Adv. Funct. Mater.*, 2007, **17**, 1873–1878.
130 H. Q. Li, R. L. Liu, D. Y. Zhao and Y. Y. Xia, *Carbon*, 2007, **45**, 2628–2635.
131 J. Yao, X. P. Shen, B. Wang, H. K. Liu and G. X. Wang, *Electrochem. Commun.*, 2009, **11**, 1849–1852.
132 D. S. Su and R. Schlogl, *ChemSusChem*, 2010, **3**, 136–168.
133 D. Y. Pan, S. Wang, B. Zhao, M. H. Wu, H. J. Zhang, Y. Wang and Z. Jiao, *Chem. Mater.*, 2009, **21**, 3136–3142.
134 P. C. Lian, X. F. Zhu, S. Z. Liang, Z. Li, W. S. Yang and H. H. Wang, *Electrochim. Acta*, 2010, **55**, 3909–3914.
135 P. Guo, H. H. Song and X. H. Chen, *Electrochem. Commun.*, 2009, **11**, 1320–1324.
136 W. Guoxiu, S. Xiaoping, J. Yao and P. Jinsoo, *Carbon*, 2009, 2049–2053.
137 A. Gerouki, M. A. Goldner, R. B. Goldner, T. E. Haas, T. Y. Liu and S. Slaven, *J. Electrochem. Soc.*, 1996, **143**, L262–L263.
138 E. Pollak, B. S. Geng, K. J. Jeon, I. T. Lucas, T. J. Richardson, F. Wang and R. Kostecki, *Nano Lett.*, 2010, **10**, 3386–3388.
139 C. Uthaisar and V. Barone, *Nano Lett.*, 2010, **10**, 2838–2842.
140 C. Y. Wang, D. Li, C. O. Too and G. G. Wallace, *Chem. Mater.*, 2009, **21**, 2604–2606.
141 A. Abouimrane, O. C. Compton, K. Amine and S. T. Nguyen, *J. Phys. Chem. C*, 2010, **114**, 12800–12804.
142 G. F. Ortiz, R. Alcantara, P. Lavela and J. L. Tirado, *J. Electrochem. Soc.*, 2005, **152**, A1797–A1803.
143 L. S. Zhang, L. Y. Jiang, H. J. Yan, W. D. Wang, W. Wang, W. G. Song, Y. G. Guo and L. J. Wan, *J. Mater. Chem.*, 2010, **20**, 5462–5467.
144 G. X. Wang, B. Wang, X. L. Wang, J. Park, S. X. Dou, H. Ahn and K. Kim, *J. Mater. Chem.*, 2009, **19**, 8378–8384.
145 H. Kim and J. Cho, *Chem. Mater.*, 2008, **20**, 1679–1681.
146 J. K. Lee, K. B. Smith, C. M. Hayner and H. H. Kung, *Chem. Commun.*, 2010, **46**, 2025–2027.
147 S. L. Chou, J. Z. Wang, M. Choucair, H. K. Liu, J. A. Stride and S. X. Dou, *Electrochem. Commun.*, 2010, **12**, 303–306.
148 D. H. Wang, R. Kou, D. Choi, Z. G. Yang, Z. M. Nie, J. Li, L. V. Saraf, D. H. Hu, J. G. Zhang, G. L. Graff, J. Liu, M. A. Pope and I. A. Aksay, *ACS Nano*, 2010, **4**, 1587–1595.
149 T. Dufaux, J. Boettcher, M. Burghard and K. Kern, *Small*, 2010, **6**, 1868–1872.
150 S. B. Yang, G. L. Cui, S. P. Pang, Q. Cao, U. Kolb, X. L. Feng, J. Maier and K. Mullen, *ChemSusChem*, 2010, **3**, 236–239.
151 Z. S. Wu, W. C. Ren, L. Wen, L. B. Gao, J. P. Zhao, Z. P. Chen, G. M. Zhou, F. Li and H. M. Cheng, *ACS Nano*, 2010, **4**, 3187–3194.
152 N. Zhu, W. Liu, M. Q. Xue, Z. A. Xie, D. Zhao, M. N. Zhang, J. T. Chen and T. B. Cao, *Electrochim. Acta*, 2010, **55**, 5813–5818.
153 K. C. Hsiao, S. C. Liao and J. M. Chen, *Electrochim. Acta*, 2008, **53**, 7242–7247.
154 A. K. Padhi, K. S. Nanjundaswamy, C. Masquelier, S. Okada and J. B. Goodenough, *J. Electrochem. Soc.*, 1997, **144**, 1609–1613.
155 K. S. Park, J. T. Son, H. T. Chung, S. J. Kim, C. H. Lee and H. G. Kim, *Electrochem. Commun.*, 2003, **5**, 839–842.
156 R. Dominko, M. Gaberscek, J. Drofenik, M. Bele and J. Jamnik, *Electrochim. Acta*, 2003, **48**, 3709–3716.
157 X. L. Li, F. Y. Kang, X. D. Bai and W. Shen, *Electrochem. Commun.*, 2007, **9**, 663–666.
158 Y. Ding, Y. Jiang, F. Xu, J. Yin, H. Ren, Q. Zhuo, Z. Long and P. Zhang, *Electrochem. Commun.*, 2010, **12**, 10–13.
159 L. Wang, H. Wang, Z. Liu, C. Xiao, S. Dong, P. Han, Z. Zhang, X. Zhang, C. Bi and G. Cui, *Solid State Ionics*, 2010, **181**, 1685–1689.
160 F. Y. Su, C. H. You, Y. B. He, W. Lv, W. Cui, F. M. Jin, B. H. Li, Q. H. Yang and F. Y. Kang, *J. Mater. Chem.*, 2010, **20**, 9644–9650.
161 E. Antolini, *J. Power Sources*, 2007, **170**, 1–12.
162 E. Antolini, *Appl. Catal., B*, 2009, **88**, 1–24.
163 P. Lu, Y. Y. Feng, X. Q. Zhang, Y. Li and W. Feng, *Science China Technological Sciences*, 2010, **53**, 2311–2319.
164 K. P. Gong, F. Du, Z. H. Xia, M. Durstock and L. M. Dai, *Science*, 2009, **323**, 760–764.
165 Y. F. Tang, B. L. Allen, D. R. Kauffman and A. Star, *J. Am. Chem. Soc.*, 2009, **131**, 13200–13201.
166 L. Qu, Y. Liu, J.-B. Baek and L. Dai, *ACS Nano*, 2010, **4**, 1321–1326.
167 Y. Y. Shao, S. Zhang, M. H. Engelhard, G. S. Li, G. C. Shao, Y. Wang, J. Liu, I. A. Aksay and Y. H. Lin, *J. Mater. Chem.*, 2010, **20**, 7491–7496.
168 A. L. Dicks, *J. Power Sources*, 2006, **156**, 128–141.
169 A. Kongkanand, S. Kuwabata, G. Girishkumar and P. Kamat, *Langmuir*, 2006, **22**, 2392–2396.
170 Y. Y. Shao, S. Zhang, C. M. Wang, Z. M. Nie, J. Liu, Y. Wang and Y. H. Lin, *J. Power Sources*, 2010, **195**, 4600–4605.
171 C. Z. Zhu, S. J. Guo, Y. M. Zhai and S. J. Dong, *Langmuir*, 2010, **26**, 7614–7618.
172 S. Liu, J. Q. Wang, J. Zeng, J. F. Ou, Z. P. Li, X. H. Liu and S. R. Yang, *J. Power Sources*, 2010, **195**, 4628–4633.
173 L. S. Zhang, X. Q. Liang, W. G. Song and Z. Y. Wu, *Phys. Chem. Chem. Phys.*, 2010, **12**, 12055–12059.
174 R. I. Jafri, N. Rajalakshmi and S. Ramaprabhu, *J. Mater. Chem.*, 2010, **20**, 7114–7117.
175 L. F. Dong, R. R. S. Gari, Z. Li, M. M. Craig and S. F. Hou, *Carbon*, 2010, **48**, 781–787.
176 L. H. Tang, Y. Wang, Y. M. Li, H. B. Feng, J. Lu and J. H. Li, *Adv. Funct. Mater.*, 2009, **19**, 2782–2789.
177 J. W. Sun, D. K. Zhong and D. R. Gamelin, *Energy Environ. Sci.*, 2010, **3**, 1252–1261.
178 R. M. Navarro, M. C. Sanchez-Sanchez, M. C. Alvarez-Galvan, F. del Valle and J. L. G. Fierro, *Energy Environ. Sci.*, 2009, **2**, 35–54.
179 A. Kudo and Y. Miseki, *Chem. Soc. Rev.*, 2009, **38**, 253–278.
180 M. D. Hernandez-Alonso, F. Fresno, S. Suarez and J. M. Coronado, *Energy Environ. Sci.*, 2009, **2**, 1231–1257.
181 I. V. Lightcap, T. H. Kosel and P. V. Kamat, *Nano Lett.*, 2010, **10**, 577–583.
182 Y. H. Ng, I. V. Lightcap, K. Goodwin, M. Matsumura and P. V. Kamat, *J. Phys. Chem. Lett.*, 2010, **1**, 2222–2227.

183 X. L. Li, X. R. Wang, L. Zhang, S. W. Lee and H. J. Dai, *Science*, 2008, **319**, 1229–1232.
184 J. K. Wassei and R. B. Kaner, *Mater. Today*, 2010, **13**, 52–59.
185 S. De, P. J. King, M. Lotya, A. O'Neill, E. M. Doherty, Y. Hernandez, G. S. Duesberg and J. N. Coleman, *Small*, 2010, **6**, 458–464.
186 S. Roth and H. J. Park, *Chem. Soc. Rev.*, 2010, **39**, 2477–2483.
187 S. Eigler, *Carbon*, 2009, **47**, 2936–2939.
188 Y. M. Shi, K. K. Kim, A. Reina, M. Hofmann, L. J. Li and J. Kong, *ACS Nano*, 2010, **4**, 2689–2694.
189 J. B. Wu, H. A. Becerril, Z. N. Bao, Z. F. Liu, Y. S. Chen and P. Peumans, *Appl. Phys. Lett.*, 2008, **92**, 263302.
190 Y. F. Xu, G. K. Long, L. Huang, Y. Huang, X. J. Wan, Y. F. Ma and Y. S. Chen, *Carbon*, 2010, **48**, 3308–3311.
191 G. Eda, Y. Y. Lin, S. Miller, C. W. Chen, W. F. Su and M. Chhowalla, *Appl. Phys. Lett.*, 2008, **92**, 233305.
192 Y. Y. Liang, J. Frisch, L. J. Zhi, H. Norouzi-Arasi, X. L. Feng, J. P. Rabe, N. Koch and K. Mullen, *Nanotechnology*, 2009, **20**, 434007.
193 C. Y. Su, Y. P. Xu, W. J. Zhang, J. W. Zhao, A. P. Liu, X. H. Tang, C. H. Tsai, Y. Z. Huang and L. J. Li, *ACS Nano*, 2010, **4**, 5285–5292.
194 Y. W. Zhu, W. W. Cai, R. D. Piner, A. Velamakanni and R. S. Ruoff, *Appl. Phys. Lett.*, 2009, **95**, 103104.
195 J. P. Zhao, S. F. Pei, W. C. Ren, L. B. Gao and H. M. Cheng, *ACS Nano*, 2010, **4**, 5245–5252.
196 I. K. Moon, J. Lee, R. S. Ruoff and H. Lee, *Nat. Commun.*, 2010, **1**, 92, DOI: 10.1038/ncomms1092.
197 D. Yang, A. Velamakanni, G. Bozoklu, S. Park, M. Stoller, R. D. Piner, S. Stankovich, I. Jung, D. A. Field, C. A. Ventrice and R. S. Ruoff, *Carbon*, 2009, **47**, 145–152.
198 M. Zhang, R. R. Parajuli, D. Mastrogiovanni, B. Dai, P. Lo, W. Cheung, R. Brukh, P. L. Chiu, T. Zhou, Z. F. Liu, E. Garfunkel and H. X. He, *Small*, 2010, **6**, 1100–1107.
199 S. Biswas and L. T. Drzal, *Nano Lett.*, 2009, **9**, 167–172.
200 S. J. Wang, Y. Geng, Q. B. Zheng and J. K. Kim, *Carbon*, 2010, **48**, 1815–1823.
201 V. C. Tung, L. M. Chen, M. J. Allen, J. K. Wassei, K. Nelson, R. B. Kaner and Y. Yang, *Nano Lett.*, 2009, **9**, 1949–1955.
202 P. J. King, U. Khan, M. Lotya, S. De and J. N. Coleman, *ACS Nano*, 2010, **4**, 4238–4246.
203 K. K. Kim, A. Reina, Y. M. Shi, H. Park, L. J. Li, Y. H. Lee and J. Kong, *Nanotechnology*, 2010, **21**, 285205.
204 C. Y. Li, Z. Li, H. W. Zhu, K. L. Wang, J. Q. Wei, X. A. Li, P. Z. Sun, H. Zhang and D. H. Wu, *J. Phys. Chem. C*, 2010, **114**, 14008–14012.
205 L. G. De Arco, Y. Zhang, C. W. Schlenker, K. Ryu, M. E. Thompson and C. W. Zhou, *ACS Nano*, 2010, **4**, 2865–2873.
206 W. W. Cai, Y. W. Zhu, X. S. Li, R. D. Piner and R. S. Ruoff, *Appl. Phys. Lett.*, 2009, **95**, 123115.
207 L. M. Goncalves, V. D. Bermudez, H. A. Ribeiro and A. M. Mendes, *Energy Environ. Sci.*, 2008, **1**, 655–667.
208 J. H. Yum, P. Chen, M. Gratzel and M. K. Nazeeruddin, *ChemSusChem*, 2008, **1**, 699–707.
209 Z. J. Ning, Y. Fu and H. Tian, *Energy Environ. Sci.*, 2010, **3**, 1170–1181.
210 T. W. Hamann, R. A. Jensen, A. B. F. Martinson, H. Van Ryswyk and J. T. Hupp, *Energy Environ. Sci.*, 2008, **1**, 66–78.
211 S. R. Sun, L. Gao and Y. Q. Liu, *Appl. Phys. Lett.*, 2010, **96**, 083113.
212 Y. B. Tang, C. S. Lee, J. Xu, Z. T. Liu, Z. H. Chen, Z. B. He, Y. L. Cao, G. D. Yuan, H. S. Song, L. M. Chen, L. B. Luo, H. M. Cheng, W. J. Zhang, I. Bello and S. T. Lee, *ACS Nano*, 2010, **4**, 3482–3488.
213 S. R. Kim, M. K. Parvez and M. Chhowalla, *Chem. Phys. Lett.*, 2009, **483**, 124–127.
214 S. Gunes, H. Neugebauer and N. S. Sariciftci, *Chem. Rev.*, 2007, **107**, 1324–1338.
215 M. Helgesen, R. Sondergaard and F. C. Krebs, *J. Mater. Chem.*, 2010, **20**, 36–60.
216 L. Valentini, M. Cardinali, S. B. Bon, D. Bagnis, R. Verdejo, M. A. Lopez-Manchado and J. M. Kenny, *J. Mater. Chem.*, 2010, **20**, 995–1000.
217 Q. Liu, Z. F. Liu, X. Y. Zhong, L. Y. Yang, N. Zhang, G. L. Pan, S. G. Yin, Y. Chen and J. Wei, *Adv. Funct. Mater.*, 2009, **19**, 894–904.
218 V. Yong and J. M. Tour, *Small*, 2010, **6**, 313–318.
219 D. Yu, Y. Yang, M. Durstock, J.-B. Baek and L. Dai, *ACS Nano*, 2010, **4**, 5633–5640.
220 S. S. Li, K. H. Tu, C. C. Lin, C. W. Chen and M. Chhowalla, *ACS Nano*, 2010, **4**, 3169–3174.
221 L. M. Dai, *ChemSusChem*, 2010, **3**, 797–799.
222 X. M. Li, H. W. Zhu, K. L. Wang, A. Y. Cao, J. Q. Wei, C. Y. Li, Y. Jia, Z. Li, X. Li and D. H. Wu, *Adv. Mater.*, 2010, **22**, 2743–2748.

